

1 **A global water cycle reanalysis (2003–2012) merging**
2 **satellite gravimetry and altimetry observations with a**
3 **hydrological multi-model ensemble**

4
5 **Albert I.J.M. van Dijk^{1*}, Luigi J. Renzullo², Yoshihide Wada³, Paul Tregoning⁴**

6
7 [1] {Fenner School of Environment & Society, The Australian National University, Canberra,
8 Australia}

9 [2] {CSIRO Land and Water, Canberra, Australia}

10 [3] {Department of Physical Geography, Utrecht University, Utrecht, Netherlands}

11 [4] {Research School of Earth Sciences, The Australian National University, Canberra,
12 Australia}

13 Correspondence to: Albert Van Dijk, albert.vandijk@anu.edu.au

14
15 **Abstract**

16 We present a global water cycle reanalysis that merges water balance estimates derived from
17 the GRACE satellite mission, satellite water level altimetry and off-line estimates from
18 several hydrological models. Error estimates for the sequential data assimilation scheme were
19 derived from available uncertainty information and the triple collocation technique. Errors in
20 four GRACE storage products were estimated to be 11–12 mm over land areas, while errors
21 in monthly storage changes derived from five global hydrological models were estimated to
22 be 17–28 mm. Prior and posterior estimates were evaluated against independent observations
23 of river water level and discharge, snow water storage and glacier mass loss. Data
24 assimilation improved or maintained agreement overall, although results varied regionally.
25 Uncertainties were greatest in regions where glacier mass loss and sub-surface storage
26 decline are both plausible but poorly constrained. We calculated a global water budget for
27 2003–2012. The main changes were a net loss of polar ice caps (-342 Gt y^{-1}) and mountain
28 glaciers (-230 Gt y^{-1}), with an additional decrease in seasonal snow pack (-18 Gt y^{-1}). Storage
29 increased due to new impoundments ($+16 \text{ Gt y}^{-1}$), but this was compensated by decreases in

30 other surface water bodies (-10 Gt y^{-1}). If the effect of groundwater depletion (-92 Gt y^{-1}) is
31 considered separately, sub-surface water storage increased by $+202 \text{ Gt y}^{-1}$ due particularly to
32 increased wetness in northern temperate regions and in the seasonally wet tropics of South
33 America and southern Africa.

34

35 **1. Introduction**

36 More accurate global water balance estimates are needed, to better understand interactions
37 between the global climate system and water cycle (Sheffield et al., 2012), the causes of
38 observed sea level rise (Boening et al., 2012; Fasullo et al., 2013; Cazenave et al., 2009;
39 Leuliette and Miller, 2009), human impacts on water resources (Wada et al., 2010; 2013), and
40 to improve hydrological models (van Dijk et al., 2011) and initialise water resources forecasts
41 (Van Dijk et al., 2013). The current generation of global hydrological models have large
42 uncertainties arising from a combination of data deficiencies (e.g., precipitation in sparsely
43 gauged regions; poorly known soil, aquifer and vegetation properties) and overly simplistic
44 descriptions of important water cycle processes (e.g. groundwater dynamics, human water
45 resources extraction and use, wetland hydrology and glacier dynamics). Data assimilation is
46 used routinely to overcome data and model limitations in atmospheric reconstructions or
47 ‘reanalysis’. In hydrological applications, there has been an (over-) emphasis on parameter
48 calibration (Van Dijk, 2011) with data assimilation approaches largely limited to flood
49 forecasting. New applications are being developed, however (Liu et al., 2012a), including
50 promising developments towards large-scale water balance reanalyses, alternatively referred
51 to as monitoring, assessment or estimation (van Dijk and Renzullo, 2011).

52 Here, we undertake a global water cycle reanalysis for the period 2003–2012. Specifically,
53 we attempt to merge global water balance estimates from different model sources with an
54 ensemble of total water storage (TWS) estimates derived from the Gravity Recovery And
55 Climate Experiment (GRACE) satellite mission (Tapley et al., 2004). Various alternative
56 approaches can be conceptualised to achieve this integration and the most appropriate among
57 these is not obvious. Our approach was to use water balance estimates generated by five
58 global hydrological models along with several ancillary data sources to generate an ensemble
59 of prior estimates of monthly water storage changes. Errors in the different model estimates
60 and GRACE products were estimated spatially through triple collocation (Stoffelen, 1998).
61 Subsequently, a data assimilation scheme was designed to sequentially merge the model
62 ensemble and GRACE observations. The reanalysis results were evaluated with independent

63 global streamflow records, remote sensing of river water level and snow water equivalent
64 (SWE), and independent glacier mass balance estimates.

65

66 **2. Methods and Data Sources**

67 **2.1. Overall approach**

68 We conceptualise TWS (S , in mm) as the sum of five different water stores (s in mm), *i.e.*,
69 water stored in snow and ice (s_{snow}); below the surface in soil and groundwater (s_{sub}), and in
70 rivers (s_{riv}); lakes (s_{lake}), and seas and oceans (s_{sea}). We ignore atmospheric water storage
71 changes, which are removed from the signal during the GRACE TWS retrieval process (e.g.,
72 Wahr et al., 2006), and vegetation mass changes, which are assumed negligible. The GRACE
73 TWS estimates are denoted by y and have the same units as S but are distinct in their much
74 smoother spatial character.

75 To date, data assimilation schemes developed for large-scale water cycle analysis typically
76 use Kalman filter approaches (Liu et al., 2012a). This requires calculation of covariance
77 matrices and, presumably because of complexity and computational burden, has only been
78 applied for single models and limited regions (e.g., Zaitchik et al., 2008). We aimed to
79 develop a data assimilation scheme that made it possible to use water balance estimates
80 derived ‘off line’ (*i.e.*, in the absence of data assimilation) so we could use an ensemble of
81 already available model outputs. In the data assimilation terminology of Bouttier and Courtier
82 (1999), our scheme could be described as sequential and near-continuous with a spatially
83 variable but temporally stable gain factor. The characteristics of the data assimilation
84 problem to be addressed in this application were as follows:

85 (1) Alternative GRACE TWS estimates (y^o) were available from different processing centres
86 and error estimates were required for each;

87 (2) Alternative estimates for some of the stores, s , were available from different hydrological
88 models, with higher definition than y^o ;

89 (3) Error estimates were required for each store and data source;

90 (4) A method was required to spatially transform between s and y as part of the assimilation.

91

92 **2.2. Data sources**

93 The data used include those needed to derive prior estimates for each of the water cycle
94 stores, the GRACE retrievals to be assimilated and independent observations to evaluate the
95 quality of the reanalysis. All are listed in Table 1 and described below.

96 Monthly water balance components from four global land surface model estimates at 1°
97 resolution were obtained from NASA’s Global Data Assimilation System (GLDAS) (Rodell
98 et al., 2004). The four models include CLM, Mosaic, NOAH and VIC which, for the 2003–
99 2012, were forced with “a combination of NOAA/GDAS atmospheric analysis fields,
100 spatially and temporally disaggregated NOAA Climate Prediction Center Merged Analysis of
101 Precipitation (CMAP) fields, and observation-based radiation fields derived using the method
102 of the Air Force Weather Agency's AGRicultural METeorological modelling system” (Rui,
103 2011). The models are described in Rodell et al. (2004). From the model outputs we used (i)
104 snow water equivalent (SWE) depth, (ii) total soil moisture storage over a soil depth that
105 varies between models, and (iii) generated streamflow, calculated as the sum of surface
106 runoff and sub-surface drainage. In addition to GLDAS, we used global water balance
107 estimates generated by the W3RA model (Van Dijk et al., 2013) in the configuration used in
108 the Asia-Pacific Water Monitor (<http://www.wenfo.org/apwm/>). For 2003–2008, the model
109 was forced with the ‘Princeton’ merged precipitation, down-welling short-wave radiation,
110 minimum and maximum daily temperature and air pressure data produced by Sheffield et al.
111 (2006). From 2009 onwards, the model primarily uses ‘ERA-Interim’ weather forecast model
112 reanalysis data from the European Centre for Medium-Range Weather Forecasts. For low
113 latitudes, these are combined with near-real time TRMM multi-sensor precipitation analysis
114 data (TMPA 3B42 RT) (Huffman et al., 2007) to improve estimates of convective rainfall
115 (Peña-Arancibia et al., 2013). Both were bias-corrected with reference to the Princeton data
116 to ensure homogeneity. W3RA model estimates were conceptually similar to those from
117 GLDAS, except that the model includes deep soil and groundwater stores and sub-grid
118 surface and groundwater routing.

119 The five hydrological models do not provide estimates of groundwater depletion and storage
120 in rivers, lakes and impoundments and these were therefore derived separately. Groundwater
121 depletion estimates were derived for 1960–2010 by Wada et al. (2012). The time series were
122 calculated as the net difference between estimated groundwater extraction and recharge.

123 National groundwater extraction data compiled by the International Groundwater Resources
124 Assessment Centre (IGRAC) were disaggregated using estimates of water use intensity and

125 surface water availability at 0.5° resolution from a hydrological model (PCR-GLOBWB; see
126 Wada et al., 2012, for details). The model also estimated recharge including return flow from
127 irrigation. Groundwater depletion uncertainty estimates were generated through 10,000
128 Monte Carlo simulations, with 100 realizations of both extraction and recharge (Wada et al.,
129 2010). This method tends to overestimate reported depletion in non-arid regions, where
130 groundwater pumping can enhance recharge from surface water. Wada et al. (2012) used a
131 universal multiplicative correction of 0.75 to account for this. Here, the correction was
132 calculated per climate region rather than world-wide, reflecting the dependency of
133 uncertainty on recharge estimates and their errors, and resulting in values of 0.6 to 0.9.
134 Depletion estimates for 2011–2012 were not available; these were estimated using monthly
135 average depletion and uncertainty values for the preceding 2003–2010 period. Given the
136 regular pattern of depletion in the preceding years this by itself is unlikely to have affected
137 the analysis noticeably.

138 River water storage was estimated by propagating runoff fields from each of the five models
139 through a global routing scheme. In a previous study, we compared these runoff fields with
140 streamflow records from 6,192 small (<10,000 km²) catchments worldwide and found that
141 observed runoff was 1.28 to 1.77 times greater than predicted by the different models (Van
142 Dijk et al., 2013). These respective values were used to uniformly bias-correct the runoff
143 fields. Next, we used a global 0.5° resolution flow direction grid (Oki et al., 1999; Oki and
144 Sud, 1998) to parameterise a cell-to-cell river routing scheme. We used a linear reservoir
145 kinematic wave approximation (Vörösmarty and Moore III, 1991), similar to that used in
146 several large-scale hydrology models (see recent review by Gong et al., 2011). The monthly
147 1° runoff fields from each of the five models were oversampled to 0.5° and daily time step
148 before routing, and the river water storage estimates (in mm) were aggregated back to
149 monthly 1° grid cell averages before use in assimilation. The routing function was an inverse
150 linear function of the distance between network nodes and a transfer (or routing) coefficient.
151 For each model, a globally uniform optimal transfer coefficient was found by testing values
152 of 0.3 to 0.9 day⁻¹ in 0.1 day⁻¹ increments and finding the value that produced best overall
153 agreement with seasonal flow patterns observed in 586 large rivers world-wide. These 586
154 were a subset of 925 ocean-reaching rivers for which streamflow records were compiled by
155 Dai et al. (2009) from various sources. We excluded locations where streamflow records
156 were available for less than 10 years since 1980 or less than 6 months of the year.

157 The resulting river flow estimates do not account for the impact of river water use (i.e., the
158 evaporation of water extracted from rivers, mainly for irrigation). We addressed this using
159 global monthly surface water use estimates that were derived in a way similar to that used for
160 groundwater depletion estimates (full details in Wada et al., 2013). For each grid cell, mean
161 water use rates for 2002–2010 were subtracted from mean runoff estimates for the same
162 period, and the remaining runoff was routed downstream. The resulting mean net river flow
163 estimates were divided by the original estimates to derive a scaling factor, which was
164 subsequently applied at each time step. Lack of additional global information on river
165 hydrology meant that three simplifications needed to be made: (i) our approach implies that
166 for a particular grid cell, monthly river water use is assumed proportional to river flow for
167 that month; (ii) the influence of lakes, wetlands and water storages on downstream flows
168 (e.g., through dam operation) is not accounted for, even though their actual storage changes
169 are (see further on); (iii) our approach does not account for losses associated with permanent
170 or ephemeral wetlands, channel leakage and net evaporation from the river channel. At least
171 in theory, data assimilation may correct mass errors resulting from these assumptions.

172 Variations in lake water storage were not modelled, but water level data for 62 lakes world-
173 wide were obtained from the Crop Explorer web site (Table 1) and include most of the
174 world's largest lakes and reservoirs, including the Caspian Sea. The water level data for these
175 lakes were derived from satellite altimetry and converted to mm water storage. Measurements
176 were typically available every 10 days. The mean and standard deviation of measurements in
177 each month were used as respectively best estimate and estimation error for that month.
178 Storage in water bodies without altimetry data was necessarily assumed negligible. This
179 includes many small lakes and dams, but also some larger lakes affected by snow and ice
180 cover (e.g., the Great Bear and Great Slave Lakes in Canada) and ephemeral, distributed or
181 otherwise complex water bodies (e.g., the Okavango delta in Botswana and Lake Eyre in
182 Australia, each of which contains $>10 \text{ km}^3$ of water when full).

183 New river impoundments lead to permanent water storage increases. A list of dams was
184 collated by Lehner et al. (2011) and was updated with large dams constructed in more recent
185 years with the ICOLD data base (Table 1). For the period 1998–2012, a total 198
186 georeferenced dams with a combined storage capacity of 418 km^3 were identified. For the
187 Three Gorges Dam (39 km^3), reservoir water level time series
188 (<http://www.ctg.com.cn/inc/sqsk.php>) were converted to storage volume following Wang et
189 al. (2011). For the remaining dams, we assumed a gradual increase to storage capacity over

190 the first five years after construction and assumed a relative estimation error of 20%. The
191 combined annual storage increase amounted to $21 \text{ km}^3 \text{ y}^{-1}$ on average.

192 Global merged mean sea level anomalies were obtained from the Aviso web site (Table 1).
193 The monthly data were reprojected from the native $1/3^\circ$ Mercator grid to regular 1° grids. An
194 estimate of uncertainty was derived by calculating the spatial standard deviation in sea level
195 values within a 4° by 4° region around each grid cell during re-projection. When sea level
196 data were missing because of sea ice, we assumed sea level did not change and assigned an
197 uncertainty of 5 mm. Following the recent global sea level budget study by Chen et al.
198 (2013), we assumed that 75% of the observed sea level change was due to mass increase, and
199 we multiplied altimetry sea level anomalies with this factor.

200 We did not have spatial global time series of glacier mass changes. The five hydrological
201 models have poor representation of ice dynamics, and therefore large uncertainties and errors
202 can be expected for glaciated regions. To account for this, we used the ‘GGHYDRO’ global
203 glacier extent mapping by Cogley (2003) to calculate the percentage glacier area for each grid
204 cell, and assumed a proportional error in monthly glacier mass change estimates
205 corresponding to 300 mm per unit glacier area. This value was chosen somewhat arbitrarily
206 but ensure that a substantial fraction of the regional analysis increment is assigned to glaciers.

207 Three alternative GRACE TWS retrieval products were downloaded from the Tellus web
208 site. The three products (coded CSR, JPL and GFZ; release 05) each had a nominal 1° and
209 monthly resolution. The land and ocean mass retrievals (Chambers and Bonin, 2012) were
210 combined. The land retrievals had been ‘de-striped’ and smoothed with a 200 km half-width
211 spherical Gaussian filter (Swenson et al., 2008; Swenson and Wahr, 2006), whereas the ocean
212 retrievals had been smoothed with a 500 km filter (Chambers and Bonin, 2012). The data
213 assimilation method we employed is designed to deal with the signal ‘leakage’ caused by the
214 smoothing process and therefore we did not use the scaling factors provided by the algorithm
215 developers. In addition, gravity fields produced by CNES/GRGS (Bruinsma et al., 2010) at 1°
216 resolution for 10 day periods were used. The three Tellus data sources had been corrected for
217 Glacial Isostatic Adjustment (GIA); we corrected the GRGS data using the same GIA
218 estimates of Geruo et al. (2013). Initial data assimilation experiments produced unexpectedly
219 strong mass trends around the Gulf of Thailand. Inspection demonstrated that all products, to
220 different degrees, contained a mass redistribution signal associated with the December 2004
221 Sumatra-Andaman earthquake. To account for this, we first calculated a time series of
222 seasonally-adjusted monthly anomalies (i.e., the average seasonal cycle was removed) for the

223 region [5°N–15°, 80–110°E]. Next, we adjusted values after December 2004 by the
 224 difference in the mean adjusted anomalies for the year before and after the earthquake,
 225 respectively.

226

227 **2.3. Data assimilation scheme**

228 For each update cycle, the data assimilation scheme proceeds through the steps illustrated in
 229 Figure 1 and described below.

230 *1) Deriving the prior estimate for each store.* The way to calculate the prior (or background)
 231 estimate of storage s_t^b varied between stores. A systematic and accumulating bias (or ‘drift’)
 232 was considered plausible for the deep soil and groundwater components of model-derived
 233 sub-surface storage due to slow groundwater dynamics (including extraction) and ice storage
 234 in permanent glaciers and ice sheets, which may be progressively melting or accumulating. In
 235 these cases, the model-estimated *change* in storage was assumed more reliable than the
 236 model-estimated storage itself, and estimates from the five models were used to calculate
 237 storage change, Δs_t^b for store i ($i=1, \dots, N$) as:

$$\Delta s_t^b(i) = \sum_{l=1}^L w_l x_t^l(i) \quad (1)$$

238 where x_t^l is the estimate of storage change from model l ($l=1, \dots, L$) between time $t-1$ and t ,
 239 and w_l the relative weight of model l in the ensemble, computed as:

$$w_l = \frac{\sigma_l^{-2}}{\sum_l \sigma_l^{-2}} \quad (2)$$

240 where σ_l is the estimated local error for model l based on triple collocation (see Section 2.4).

241 Subsequently, s_t^b was calculated as:

$$s_t^b(i) = s_{t-1}^{a*}(i) + \Delta s_t^b(i) \quad (3)$$

242 where s_{t-1}^{a*} is the posterior (or analysis) estimate from the previous time step. This approach
 243 was not suitable for model-estimated seasonal snowpack and river storage, where the
 244 ephemeral nature of the storage means that long-term drift is not an issue and Eq. (2) could in
 245 fact lead to unrealistic negative storage values. For these cases, s_t^b was computed as:

$$s_t^b(i) = \sum_{l=1}^L w_l s_t^l(i) \quad (4)$$

246 where s_t^l is the storage estimate from model l . The glacier extent map was used to identify
 247 whether Eq. (3) or (4) should be used for s_{snow} . Similarly, no drift was expected in the ocean
 248 and lake storage data, and these were used directly as estimates of s_t^b .

249 2) *Deriving the prior estimate of GRACE-like TWS (y^b)*. This estimate was derived by
 250 summing all stores s_t^b as:

$$S_t^b = \sum_{i=1}^N s_t^b(i) \quad (5)$$

251 and subsequently applying a convolution operator Γ to transform S_t^b to a ‘GRACE-like’ TWS
 252 y^b . The operator Γ was a Gaussian smoother (cf. Jekeli, 1981) written here as:

$$y_t^b(j_1) = \sum_{j_2} \Gamma(j_1, j_2) S_t^b(j_1, j_2) \quad (6)$$

253 where j_1 and j_2 in principle should encompass all existing grid cell coordinates. In practice, Γ
 254 was applied as a moving Gaussian kernel with a size of $6^\circ \times 6^\circ$ and a half-width of 300 km
 255 (see further on).

256 3) *Updating the GRACE-like TWS*. The updated GRACE-like TWS, y_t^a , was calculated from
 257 the prior (Eq. (6)) and GRACE observations y_t^o for time t as (cf. Figure 1 a-d):

$$y_t^a = y_t^b + \delta y_t = y_t^b + k(y_t^o - y_t^b) \quad (7)$$

258 where δy_t is the analysis increment and k a temporally static gain factor derived by
 259 combining the error variances of modelled and observed y as follows:

$$k = \frac{\sum_l w_{y,l} \sigma_{y,l}^2}{\sum_l w_{y,l} \sigma_{y,l}^2 + \sum_m w_{y,m} \sigma_{y,m}^2} \quad (8)$$

260 where $w_{y,l}$ and $w_{y,m}$ are the weights applied to each of the five GRACE-like TWS estimates
 261 and four GRACE data sources, respectively, calculated from their respective error variances
 262 $\sigma_{y,l}^2$ and $\sigma_{y,m}^2$ analogous to Eq. (2).

263 4) *Spatially disaggregating the analysis increment to the different stores*. The observation
 264 model was inverted and combined with the store error estimates in order to spatially
 265 redistribute the analysis increment δy_t , as follows (cf. Figure 1e-g):

$$\delta s_t(i, j_1) = \sum_{j_2} \Omega(j_1, j_2) \delta y_t(j_2) \quad (9)$$

266 where the redistribution operator Ω can be written as (cf. Figure 1g):

$$\Omega(j_1, j_2) = \frac{\Gamma(j_1, j_2) \sigma^{-2}(i, j_2)}{\sum_i \sum_{j_1} \Gamma(j_1, j_2) \sigma^{-2}(i, j_2)} \quad (10)$$

267 To implement this, spatial error estimates are required for each store. For lakes and seas, the
 268 errors were estimated from the observations (see Section 2.2). For the model-based estimates,
 269 the error was calculated for each time step and store as:

$$\sigma_t^2(i) = \sum_l w_l [x_t^l(i) - \Delta s_t^b(i)]^2 \quad (11)$$

270 The resulting error estimates are spatially and temporally dynamic and respond to the
 271 magnitude of the differences between the different model estimates. For s_{sub} and s_{snow} we
 272 combined the error estimates derived by Eq. (11) with the estimated errors in groundwater
 273 depletion and glacier mass change, respectively (see Section 2.2), calculating total error as
 274 the quadratic sum of the composite errors.

275 5) *Updating the stores.* In the final step, the state of each store is updated:

$$s_t^a(i) = s_t^b(i) + \delta s_t(i) \quad (12)$$

276 Subsequently, the procedure is repeated for the next time step.

277

278 **2.4. Error estimation**

279 Spatial error fields are required for all data sets to calculate the gain factor k . Where
 280 necessary these were estimated using the triple collocation technique (Stoffelen, 1998). This
 281 technique infers errors in three independent time series by analysing the covariance structure.
 282 The approach has been applied widely to estimate errors in, among others, satellite-derived
 283 surface soil moisture (Dorigo et al., 2010; Scipal et al., 2009), evapotranspiration (Miralles et
 284 al., 2011) and vegetation leaf area (Fang et al., 2012). A useful description of the technique,
 285 the assumptions underlying it and an extension of the theory to more than three time series is
 286 provided by Zwieback et al. (2012). Application requires three (or more) estimates of the
 287 same quantity. This was achieved by convolving the model-derived storage estimates into
 288 large-scale, smoothed TWS estimates equivalent to those derived from GRACE
 289 measurements using Eqs. (5) and (6). Inspection of the original Tellus data made clear that

290 the 200 km filter that was already applied as part of the land retrieval had only removed part
291 of the spurious aliasing in the data sets, and propagated these artefacts into the error estimates
292 and reanalysis. Therefore a smoother, 300 km filter was applied to the Tellus TWS data sets.
293 Because conceptual consistency is required for triple collocation, the same filter was applied
294 to the GRGS and model-derived TWS estimates. Several alternative Tellus and model time
295 series were available, and therefore the triple collocation technique could be used to produce
296 alternative error estimates from multiple triplet combinations (i.e., five for Tellus TWS, three
297 for model TWS, and $5 \times 3 = 15$ for GRGS TWS). The agreement between these alternative
298 estimates was calculated as a measure of uncertainty in the estimated errors.

299 Important assumptions of the collocation technique are that: (1) each data set is free of bias
300 relative to each other, (2) errors do not vary over time, (3) there is no temporal
301 autocorrelation in the errors, and (4) there is no correlation between the errors in the
302 respective time series (Zwieback et al., 2012). Each of these assumptions is difficult to
303 ascertain, but some interpretative points can be made. Errors in the GRACE products vary
304 somewhat from month to month depending on data availability, and overall decreased after
305 June 2003. Therefore assumption (2) is a simplification.

306 Assumption (3) is also unlikely to hold fully for the TWS estimates themselves: there will
307 almost certainly be systematic errors and biases that cause temporal correlation in the errors
308 in the modelled TWS (e.g., due to poorly represented processes causing secular trends such
309 as groundwater extraction or glacier melt). We were able to avoid this assumption by
310 applying the triple collocation to monthly storage changes rather than the actual value of
311 storage, although temporal correlation in storage change errors remains a possibility.

312 Temporal correlation in the GRACE errors is unlikely, however. Therefore, the error in
313 individual monthly mass estimates was calculated following conventional error propagation
314 theory by dividing the estimated error in mass changes by $\sqrt{2}$.

315 Assumption (4) will not be fully met where estimates are partially based on the same
316 principle or measurement. In this study, arguably the most uncertain assumption is that the
317 GRGS and Tellus errors are to a large extent uncorrelated. The basis for this assumption is
318 that most of the error is likely to derive from the TWS retrieval method rather than the
319 primary measurements (Sakumura et al., 2014). The GRGS time series was selected as the
320 third triple collocation member because the four Tellus products are retrieved by methods
321 that are comparatively more similar than the GRGS method, which uses ancillary
322 observations from the Laser Geodynamics Satellites (Tregoning et al., 2012).

323 Correspondingly, global average correlation among the Tellus TWS time series was stronger
324 (0.61–0.73) than between GRGS and any of the Tellus time series (0.49–0.58). Nonetheless,
325 there may well have been a residual covariance between errors in the GRGS and Tellus
326 products. In triple collocation and subsequent data assimilation, this would cause some part
327 of the differences to be wrongly attributed to the prior estimates rather than the observation
328 products. Therefore, we conservatively inflated the calculated value by including an
329 additional error of 5 mm through quadratic summation before calculating the gain factor (Eq.
330 8).

331 Uncertainty in the derived error estimates also arises from sample size, i.e. the number of
332 collocated observations ($N=111$). Previous studies have suggested that 100 samples are
333 sufficient to produce a reasonable estimate (Dorigo et al., 2010), although Zwieback et al.
334 (2012) calculate that the relative uncertainty in the estimated errors for $N=111$ can be
335 expected to be in the order of 20%. An uncertainty of this magnitude will not have a strong
336 impact on the reanalysis results.

337

338 **2.5. Evaluation against observations**

339 Evaluation of the reanalysis results for sub-surface storage was a challenge: ground
340 observations are not widely available at global scale, are not conceptually equivalent to the
341 reanalysis terms, require tenuous scaling assumptions for comparison at 1° grid cell
342 resolution, and many existing data sets contain few or no records during 2003–2012. For
343 example, comparison with in situ soil moisture measurements or groundwater bore data is
344 beset by such problems (Tregoning et al., 2012). Similarly, an initial comparison with near-
345 surface (<5 cm depth) soil moisture estimates from passive and active microwave remote
346 sensing (Liu et al., 2012b; Liu et al., 2011) showed that the conceptual difference between the
347 two quantities was too great for any meaningful comparison.

348 We were able to evaluate the reanalysis for storage in rivers, seasonal snow pack and
349 glaciers, however. Firstly, a total of 1,264 water level time series for several large rivers
350 worldwide were obtained from the Laboratoire d'Etudes en Géodésie et Océanographie
351 Spatiales (LEGOS) HYDROWEB web site (Table 1). The river levels were retrieved from
352 ENVISAT and JASON-2 satellite altimetry (Créaux et al., 2011) and included uncertainty
353 information for each data period. From each time series, we removed data points with an
354 estimated error of more than 25% of the temporal standard deviation (SD). Another 165

355 altimetry time series were obtained from the European Space Agency (ESA) River&Lake
356 web site (Berry, 2009). These were selected to increase measurement period and sample size
357 for the available locations, as well as extending coverage to additional rivers. The ESA time
358 series did not include error estimates; instead data plots were judged visually to assess the
359 likelihood of measurement noise; seemingly affected time series and outlier data points
360 ($>3SD$) were excluded. The total 1,429 time series were merged for individual 1° grid cells.
361 In each case, the longest time series was chosen as reference. Overlapping time periods were
362 used to remove (typically small) systematic biases in water surface elevation between time
363 series; where there was no overlap the time series were normalised by the median water level.
364 The ESA data were used where or when HYDROWEB data were not available, and merged
365 time series with fewer than 24 data points in total were excluded. The resulting data set
366 contained time series for 442 grid cells with an average 61 (maximum 115) data points during
367 2003–2012. The relationship between river water level and river discharge (i.e., the discharge
368 rating curve) was unknown, and therefore a direct comparison could not be made. The
369 relationship is typically non-linear, and therefore we calculated Spearman's rank correlation
370 coefficient (ρ) between estimated discharge and observed water level.

371 Secondly, we used the already mentioned discharge data for 586 ocean-reaching rivers world-
372 wide (Dai et al., 2009). From these, we selected 430 basins for which the reported drainage
373 area was within 20% of the area derived from the 0.5° routing network. The ratio between
374 reported and model-derived drainage area was used to adjust the reanalysis estimates and
375 these were compared with recorded mean streamflow. The recorded mean annual discharge
376 values are not for 2003-2012, but we assume that the differences are not systematic and,
377 therefore, that any large change in agreement may still be a useful indicator of reanalysis
378 quality.

379 Third, snow storage estimates were evaluated with the ESA GlobSnow product (Luoju et al.,
380 2010). This data set contains monthly 0.25° resolution estimates of snow water equivalent
381 (SWE, in mm) for low relief regions with seasonal snow cover north of $55^\circ N$ during 2003–
382 2011. The SWE estimates are derived through a combination of AMSR-E passive microwave
383 remote sensing and weather station data (Pulliainen, 2006; Takala et al., 2009). The
384 GlobSnow data were aggregated to 1° resolution. The root mean square error (RMSE) and
385 the coefficient of correlation (r^2) were calculated as measures of agreement.

386 Finally, we compared the estimated trends in storage in different glacier regions to trends for
387 mountain glaciers compiled by Gardner et al. (2013) for 2003–2010 and for Greenland and

388 Antarctica by Jacob et al. (2012) for 2003–2009. In several cases these mass balance
389 estimates were based on independent glaciological or ICESAT satellite observations and
390 these were the focus of comparison. Other estimates were partially or wholly based on
391 GRACE data, making comparison less insightful.

392

393 **3. Results**

394 **3.1. Error estimation**

395 The mean errors derived by the triple collocation technique were of similar magnitude for the
396 GRACE and model estimates (Table 2; note that the numbers listed are for storage change
397 rather than storage per se and were not yet adjusted for GRACE error covariance; cf. Section
398 2.4). The relatively low values for the coefficient of variation suggest that the error estimates
399 are reasonably robust.

400 The spatial error in merged GRACE and model storage change estimates were calculated
401 analogous to Eq. (8). The resulting GRACE error surface was relatively homogeneous with
402 an estimated error of around 5–20 mm for most regions, but increasing to 20–40 mm over
403 parts of the Amazon and the Arctic (Figure 2a). The combined model error surface suggest
404 that errors are smaller than those in the GRACE data for arid regions (<10 mm) but higher
405 elsewhere, increasing beyond 80 mm in the Amazon region (Figure 2b). The mean errors
406 over non-glaciated land areas were similar, at 18.1 mm for the combined model and 13.5 mm
407 for the combined GRACE data. Assuming no temporal correlation and allowing for error
408 covariance among GRACE products reduces the latter to 10.8 mm (i.e., $\sqrt{13.5^2/2 + 5^2}$).

409

410 **3.2. Analysis increments**

411 Inspection of the analysis increments and the overall difference between prior and posterior
412 estimates provides insights into the functioning of the assimilation scheme (Figure 3). The
413 spatial pattern in root mean squared (RMS) TWS increments ($\sqrt{\delta S^2}$) emphasises the
414 important role of the world's largest rivers in explaining mismatches between expected and
415 observed mass changes, particularly in tropical humid regions (Figure 3a). Large increments
416 also occurred over Greenland (mainly due to updated ice storage changes) and the seasonally-
417 wet regions of Brazil, Angola and south Asia (sub-surface storage). When considering the
418 RMS between prior and posterior estimates of actual TWS as opposed to monthly changes

419 (Figure 3b) a similar pattern emerges, but with more emphasis on the smaller but
420 accumulating difference in estimated storage over Greenland, Alaska and part of Antarctica
421 (due to updated ice mass changes) and northwest India (groundwater depletion).

422

423

424 **3.3. Mass balance and trends**

425 At global scale, the trend and monthly fluctuations (expressed in standard deviation, SD) in
426 mean total water mass should be close to zero, allowing for small changes in atmospheric
427 water content. This provides a test of internal consistency. Among the original GRACE TWS
428 data, the GRGS data showed the smallest temporal SD (0.04 mm) and linear trend ($0.007 \pm$
429 0.001 SD mm y^{-1}) in global water mass. The three Tellus retrievals showed larger temporal
430 SD (4.7–6.4 mm) and trends (-0.37 ± 0.21 to -0.23 ± 0.20 mm y^{-1}). The merged GRACE
431 TWS data had intermediate SD (3.97 mm) and trend (-0.32 mm y^{-1}). Assimilation reduced
432 SD (to 3.1 mm) and removed the residual trend (-0.01 ± 0.10 mm y^{-1}). The discrepancies in
433 global water mass trends in the merged GRACE data and in the analysis were mostly located
434 over the oceans, and therefore the achieved mass balance closure can be attributed to the
435 influence of the prior sea mass change estimates, specifically, the conversion between sea
436 level and mass change (Figure 4).

437

438 **3.4. Regional storage trends**

439 The spatial pattern in linear trends in the merged GRACE TWS (y_0) and the reanalysis signal
440 (y_b) agree well (Figure 4bc), suggesting that the assimilation scheme is able to merge the
441 prior estimates of storage changes and observed storage as intended. Seasonally adjusted
442 anomalies were calculated for the prior and posterior estimates of the different water cycle
443 components by subtracting the mean seasonal pattern. The 2003–2012 linear trends in these
444 adjusted anomalies (Figure 5) show that the analysis has (i) increased spatial variability in
445 sub-surface water storage trends, with amplified increasing and decreasing trends (Figure
446 5ab); (ii) drastically changes trends in snow and ice storage and typically made them more
447 negative (Figure 5cd); (iii) reversed river water storage trends in the lower Amazon and
448 Congo Rivers (Figure 5ef). The reanalysis shows a complex pattern of strongly decreasing
449 and increasing sub-surface water storage trends in northwest India (Figure 5b). This may be
450 an artefact from incorrectly specified errors in the groundwater depletion estimates (see
451 Section 4.2). Less visible is that the analysis often reduced negative storage trends in other

452 regions with groundwater depletion, that is, decreased the magnitude of estimated depletion.
453 Because all sub-surface storage terms were combined, an alternative estimate of groundwater
454 depletion cannot be calculated directly, but it can be estimated: for all grid cells with significant
455 prior groundwater depletion estimates ($>0.5 \text{ mm y}^{-1}$, representing 99% of total global
456 groundwater depletion) the 2003–2012 trend in sub-surface storage change was estimated a
457 priori at $-168 \pm 3 \text{ (SD) km}^3 \text{ y}^{-1}$ of which 157 km^3 (94%) due to groundwater depletion and the
458 remaining -11 km^3 due to climate variability. Analysis reduced the total trend for these grid
459 cells to $-103 \pm 3 \text{ km}^3$ per year, from which an alternative groundwater extraction estimate of
460 ca. 92 km^3 can be derived.

461 From the seasonally adjusted anomalies, time series and trends of global storage in different
462 water cycle components were calculated. We calculated snow and ice mass change separately
463 for regions with seasonal snow cover, high ($>55^\circ$) latitude glaciers, and remaining glaciers
464 (Figure 6). The mean 2003–2012 trends are listed in Table 3; for the posterior estimates also
465 as equivalent sea level rise (SLR, by dividing by the fraction of Earth's surface occupied by
466 oceans, i.e., 0.7116) and volume ($\text{km}^3 \text{ y}^{-1}$, equivalent to Gt y^{-1}). Some of the effects of the
467 assimilation were to (i) remove the decreasing trend in prior global terrestrial sub-surface
468 water storage estimates (Figure 6a), (ii) change the poor prior estimates of polar ice cap mass
469 considerably (Figure 6fg), (iii) reduce the estimated rate of ocean mass increase from $1.84 \pm$
470 0.06 (SD) mm to $1.45 \pm 0.05 \text{ mm}$ (Table 3), and (iv) achieve mass balance closure between net
471 terrestrial and ocean storage changes (cf. Section 3.3).

472

473 **3.5. Evaluation against river level remote sensing**

474 The rank correlation (ρ) between river water level and estimated discharge for the 445 grid
475 cells with altimetry time series are shown in Figure 7. Overall there was no significant change
476 in agreement between the prior ($\rho = 0.63 \pm 0.27 \text{ SD}$) and posterior ($\rho = 0.63 \pm 0.26$)
477 estimates, with an average change of $+0.01 \pm 0.12$. However, ρ did improve for more
478 locations than it deteriorated (286 vs. 159). There are some spatial patterns in the influence of
479 assimilation (Figure 7c): strong improvements in the northern Amazon and Orinoco basins
480 and most African rivers, except for some stations along the Congo and middle Nile Rivers,
481 and reduced agreement for rivers in China (where prior estimates agreed well) and most
482 stations in the Paraná and Uruguay basins (where they did not). In most remaining rivers,
483 agreement did not change much; in some cases because it was already very good (e.g., the
484 Ganges-Brahmaputra and remainder of the Amazon basin). Altimetry and estimated

485 discharge time series are shown in Figure 8 for grid cells with the most data points in three
486 large river systems. In these cases, there is reasonably clear improvement in agreement.

487

488 **3.6. Evaluation against historic river discharge observations**

489 The prior estimate of discharge (i.e., the error-weighted average of the four bias-corrected
490 models) provided estimates that were already considerably better than any of the individual
491 members (Table 4, Figure 9). Assimilation led to small improvements in RMSE, from 47 to
492 $44 \text{ km}^3 \text{ y}^{-1}$, and a slight deterioration in the median absolute percentage difference from 40 to
493 41%. Combined recorded discharge from the 430 selected basins was $20,909 \text{ km}^3 \text{ y}^{-1}$,
494 representing 90% of estimated total discharge to the world's oceans according to Dai et al.
495 (2009). Assimilation improved the agreement with this number from -11% to -4%, of which
496 about half (5%) is due to a closer estimate of Amazon River discharge. However, modelled
497 and observed discharge values relate to different time periods and so it is not clear whether
498 this should be considered evidence for improvement or merely reflects multi-annual
499 variability.

500

501 **3.7. Evaluation against snow water equivalent remote sensing**

502 The spatial RMSE and correlation between the prior and posterior SWE estimates and the
503 GlobSnow retrievals are shown in Figure 10. Although RMSE deteriorated in a majority
504 (57%) of grid cells, correlation remained unchanged at $R^2=0.79$ and average RMSE improved
505 slightly from 23.2 to 22.3 mm. Assimilation appeared most successful for grid cells with
506 large prior RMSE in northern Canada (Figure 10a-c).

507

508 **3.8. Evaluation against glacier mass balance estimates**

509 Glacier mass changes reported in the literature (Gardner et al., 2013; Jacob et al., 2012) are
510 listed in Table 5 and compared to regional mass trends associated with glaciers and other
511 components of the terrestrial water derived from the analysis. In the polar regions (e.g.,
512 Antarctica, Greenland, Iceland, Svalbard, and the Russian Arctic) a large part of the gravity
513 signal is necessarily from glacier mass change. Published trends for most of these regions
514 also heavily rely on GRACE data and hence our estimates are generally in good agreement.
515 Remaining differences can be attributed to the products, product versions and post-processing
516 methods used, without providing insight into the accuracy of our analysis estimates. In the

517 other regions, the glaciated areas are smaller and surrounded by ice-free terrain, which
518 strongly increases the potential for incorrect distribution of analysis increments, as evidenced
519 by the high trend ratios (>47%, last column Table 5). As a consequence, glacier mass trends
520 are not well constrained by GRACE data alone and alternative observations are required. The
521 agreement with independently derived trend estimates varies. For the Canadian Arctic
522 Archipelago, Alaska and adjoining North America, the assimilation scheme assigns only 55%
523 (68 Gt y^{-1}) of the total regional negative mass trend (-124 Gt y^{-1}) to glacier mass changes,
524 with most of the remainder (40% or 50 Gt y^{-1}) assigned to sub-surface water storage changes.
525 Excluding regions for which independent storage change estimates are not available
526 (Greenland, Antarctica and Patagonia), our estimate of total glacier storage change in the
527 world's glaciers ($-114 \text{ km}^3 \text{ y}^{-1}$) was $101 \text{ km}^3 \text{ y}^{-1}$ less than the estimate of Gardner et al. (2013)
528 ($-215 \text{ km}^3 \text{ y}^{-1}$).

529

530 **4. Discussion**

531 **4.1. Estimated errors**

532 The triple collocation method produced estimates of errors in month-to-month changes in
533 GRACE TWS estimates of 12.8–14.3 mm over non-glaciated land areas. From these,
534 GRACE TWS errors of 10.4–12.0 mm can be estimated (cf. Section 3.1). By comparison,
535 reported uncertainty estimates based on formal error propagation are larger, usually in the
536 order of 20–25 mm (e.g., Landerer and Swenson, 2012; Tregoning et al., 2012; Wahr et al.,
537 2006). One possible explanation is that the 5 mm we assumed to correct for potential
538 covariance in errors between the GRACE products is too low, another that the formal
539 uncertainty estimates are too conservative. Inflating the GRACE error estimates by 10 mm
540 instead of 5 mm reduced the gain by 18% on average. The resulting uncertainty in the
541 analysis is modest (see next section). Formal error analyses predict that the retrieval errors
542 decrease towards the poles due to the closer spacing of satellite overpasses (Wahr et al.,
543 2006), but we did not find such a latitudinal pattern.

544 The mean errors in monthly changes in prior TWS for the different models were 16.5–27.9
545 mm. We do not have independent estimates of errors in modelled large-scale TWS with
546 which to compare, but the estimates would seem plausible and perhaps less than we
547 anticipated. From a theoretical perspective, violation of the assumptions underpinning triple
548 collocation is likely to have produced overestimates of model error, if anything. The
549 calculated error in the prior estimates over oceans and very stable regions such as Mongolia

550 and the Sahara are around 5 mm (Figure 2). This provides some further evidence to suggest
551 that the 5 mm GRACE error inflation we applied may have been reasonable. The largest
552 errors in the merged model estimates (>40 mm) were found for humid tropical regions and
553 high latitudes. The former may be attributed to the combination of large storage variations
554 and often uncertain rainfall estimates. Precipitation measurements are also fewer at high
555 latitudes, while poor prediction of snow and ice dynamics and melt water river hydrology are
556 also likely factors.

557

558 **4.2. Assimilation scheme performance**

559 The spatial pattern in analysis increments emphasises the importance of water stores other
560 than the soil in explaining discrepancies between model and GRACE TWS estimates (Figure
561 3). Adjustments to storage changes in large rivers, groundwater depletion, mass changes in
562 high latitude ice caps and glaciers (e.g., Greenland, Alaska and Antarctica) and lake water
563 levels (e.g., the Caspian Sea and the North-American Great Lakes) were all considerable
564 within their region, absorbing monthly analysis increments, long-term trend discrepancies, or
565 both.

566 Uncertainty in error estimates for the different data sources affects the analysis in different
567 ways. Incorrect estimation of GRACE and model-derived TWS errors by the triple
568 collocation method primarily affects (i) the weighting of the ensemble members and (ii) the
569 gain matrix. Appropriate weighting only requires that the relative magnitude of errors among
570 ensemble members is estimated correctly (cf. Eq. (2)). The average errors for the different
571 GRACE TWS estimates were all within 14% of the ensemble average (Table 2) and did not
572 have strong spatial patterns, and therefore the analysis would likely have been very similar if
573 equal weighting had been applied (cf. Sakumura et al., 2014). Estimated model errors showed
574 greater differences (up to 52% greater than the ensemble mean, Table 2) as well as regional
575 patterns. However, the relative rankings and their spatial pattern were robust to the choice of
576 GRACE TWS members in triple collocation, as evidenced by a low coefficient of variation in
577 error estimates (Table 2). This suggests that the errors were correctly specified in a relative
578 sense. For the gain matrix, the relative magnitude of errors in GRACE *versus* model TWS
579 ensemble means needed to be estimated correctly (cf. Eq. (8)). The estimated GRACE TWS
580 ensemble errors are reasonably homogeneous in space (Figure 1a) which increases our
581 confidence in their validity. The uncertainty due to the correction for assumed correlation
582 between the GRGS and Tellus TWS (see previous section) is further mitigated by the design

583 of the data assimilation scheme: the gain factor determines how rapidly the analysis
584 converges towards the GRACE observations and therefore is important for month-to-month
585 variations, but long-term trends in TWS will always approach those in the GRACE
586 observations (cf. Figure 4b and c).

587 The main sources of uncertainty in long-term trends in the individual water balance terms are
588 (i) the removal of non-hydrological mass trends in the GRACE TWS time series and (ii)
589 accurate specification of relative errors in the individual water balance terms, which is needed
590 for correct redistribution of the integrated TWS analysis increments. For example, the
591 analysis results illustrate the insufficiently constrained problem of separating gravity signals
592 due to mass changes in mountain glaciers from nearby sub-surface water storage changes.
593 This was particularly evident around the Gulf of Alaska and northwest India, where decreases
594 can be expected not only in glacier mass but also in sub-surface storage due to, respectively, a
595 regional drying trend and high groundwater extraction rates (Figure 5a). We suspect that
596 unexpectedly strong increasing storage trends in parts of northwest India may be because the
597 prior groundwater depletion estimates were too high and the assigned errors too low, causing
598 the analysis update to distribute increments incorrectly. We could have addressed this by
599 inflating the local groundwater depletion estimation errors, but more research is needed to
600 understand the underlying causes. Plausible causes are that groundwater extraction is
601 overestimated, or that extraction is compensated by induced groundwater recharge (e.g., from
602 connected rivers) (see Wada et al., 2010 for further discussion).

603 Mass balance closure was not enforced and hence provides a useful diagnostic of reanalysis
604 quality. The GRGS product achieved approximate global mass balance closure at all time
605 scales, but the three Tellus products showed a seasonal cycle and long-term negative trend in
606 global water mass. Accounting for atmospheric water vapour mass changes (from ERA-
607 Interim reanalysis and the NVAP-M satellite product, data not shown) could not explain the
608 trends and in fact slightly increased the seasonal cycle in global water mass. Data
609 assimilation reduced the seasonal cycle and entirely removed the trend in total water mass,
610 thanks to the prior estimates of sea mass increase. For comparison, we calculated average
611 ocean mass increases by an alternative, more conventional method, which involved avoiding
612 areas likely to be affected by nearby land water storage changes. Excluding a 1000 km buffer
613 zone produced a 2003–2012 mass trend of +0.58 to +0.72 mm y⁻¹ for the three Tellus
614 retrievals, +1.12 mm y⁻¹ for the GRGS retrieval, and +0.75 mm y⁻¹ for the merged GRACE
615 data. Data assimilation produced a stronger trend of +1.22 mm y⁻¹ due to the influence of the

616 prior estimate of $+1.67 \text{ mm y}^{-1}$. Our prior estimate followed Chen et al. (2013), who used an
617 iterative modelling approach to attribute 75% of altimetry-observed SLR to mass increase.
618 Chen et al. (2013) argue that the conventional method produces underestimates of ocean mass
619 increase. Indeed, the trends we calculated for the ‘buffered’ ocean regions are lower than for
620 the entire oceans ($+1.22$ vs. $+1.45 \text{ mm y}^{-1}$ for the reanalysis, and $+1.67$ vs. $+1.84 \text{ mm y}^{-1}$ for
621 the prior estimates; Table 3). Nonetheless, the reduction in sea mass change of 0.39 mm y^{-1}
622 from prior to analysis does appear to reopen the problem of reconciling mass and temperature
623 observations with the altimetry derived mean sea level rise of $+2.45 \pm 0.08 \text{ mm y}^{-1}$ (cf. Chen
624 et al., 2013).

625

626 **4.3. Evaluation against observations**

627 The reanalysis generally did not have much impact on the agreement with river and snow
628 storage observations, with small improvements for some locations and small degradations for
629 others. While a robust increase in the agreement would have been desirable, the fact that
630 agreement was not degraded overall was encouraging. The data assimilation procedure
631 applied has the important benefit of bringing the estimates into agreement with GRACE
632 observations. Moreover, performance improvements with respect to river discharge and level
633 data did occur in the Amazon, where they make an important contribution to TWS changes.
634 Similarly, snow water equivalent estimates were improved in the North-American Arctic,
635 where errors in the prior estimates were largest. This demonstrates that GRACE data can
636 indeed be successfully used to constrain water balance estimates, although further
637 development may be needed to avoid some of the undesired performance degradation for
638 water balance components that do not contribute much to the TWS signal.

639 The models used for our prior estimates provided poorly constrained estimates of ice mass
640 balance changes, and our reanalysis ice mass loss estimates should not be assumed more
641 accurate than estimates based on more direct methods (Table 5). Our analysis is unique when
642 compared to previous estimates based on GRACE, in that data assimilation allowed some of
643 the observed mass changes to be attributed to other water balance components within the
644 same region, depending on relative uncertainties in the prior estimates. Comparison against
645 independent estimates of glacier mass balance changes also demonstrated the challenge of
646 correct attribution, however. Glacier mass balance estimates were in good agreement for
647 several regions, but estimates for North American glaciers in particular were questionable:
648 their combined mass loss (-68 Gt y^{-1}) was much lower than the estimates derived by

649 independent means (-124 Gt y^{-1} ; Table 5). This can be explained by incorrect specification of
650 errors. Two caveats are made: (i) the GIA signal is relatively large for these three regions
651 ($+50 \text{ Gt y}^{-1}$) and hence GIA estimation errors may have had an impact; and (ii) a significant
652 change in sub-surface water storage is plausible in principle; for example, higher summer
653 temperatures could be expected to enhance permafrost melting and runoff, as well as enhance
654 evaporation. More accurate spatiotemporal observation and modelling of glacier dynamics
655 are needed to reduce this uncertainty.

656

657 **4.4. Contributions to sea level rise**

658 The reanalysis estimate of net terrestrial water storage change of -495 Gt y^{-1} (Table 3)
659 appears a plausible estimate of ocean mass change, equivalent to ca. $+1.4 \text{ mm y}^{-1}$ sea level
660 rise. Our results confirmed that mass loss from the polar ice caps is the greatest contributor to
661 net terrestrial water loss, with Antarctica and Greenland together contributing -342 Gt y^{-1} .
662 The next largest contribution was from the remaining glaciers. We combine the reanalysis
663 estimate of -129 Gt y^{-1} with another -101 Gt y^{-1} estimated to be misattributed (cf. Section 3.8)
664 and obtain an alternative estimate of -230 Gt y^{-1} . A small but significant contribution of -18
665 Gt y^{-1} (Table 3) was estimated to originate from reductions in seasonal snow cover
666 (particularly in Quebec and Siberia; Figure 5cd). Inter-annual changes in river water storage
667 were not significant. Small contributions of -10 Gt y^{-1} and $+16 \text{ Gt y}^{-1}$ were attributed to
668 storage changes in existing lakes and large new dams, respectively, and compensated each
669 other. The largest change in an individual water body was in the Caspian Sea (-27 Gt y^{-1} , cf.
670 Figure 5) which experiences strong multi-annual water storage variations depending on
671 Volga River inflows.

672 Finally, the analysis suggested a statistically insignificant change of $+9 \text{ Gt y}^{-1}$ in sub-surface
673 storage globally. Adding back the suspected misattribution of 101 Gt y^{-1} associated with
674 glaciers produces an alternative estimate of $+110 \text{ Gt y}^{-1}$ (cf. Figure 6a). Combining this with
675 the -92 Gt y^{-1} attributed to groundwater depletion suggests that storage over the remaining
676 land areas increased by 202 Gt y^{-1} . Calculating sub-surface storage trends by latitude band
677 suggests that most of the terrestrial water ‘sink’ can be found north of 40°N and between 0 –
678 30°S and is opposite to the prior estimates (Figure 11). The main tropical regions
679 experiencing increases are in the Okavango and upper Zambezi basins in southern Africa and
680 the Amazon and Orinoco basins in northern South America (Figure 5b). Storage increases for
681 these regions are also evident from the original GRACE data (Figure 4a) and cannot be

682 attributed to storage changes in rivers or large lakes. The affected regions contain low relief,
683 poorly drained areas with (seasonally) high rainfall. In such environments, the storage
684 changes could occur in the soil, groundwater, wetlands, or a combination of these. Further
685 attribution is impossible without additional constraining observations (Tregoning et al., 2012;
686 van Dijk et al., 2011). The ten-year analysis period is short and this cautions against over-
687 interpreting this apparent ‘tropical water sink’. However it is of interest to note that a gradual
688 strengthening of global monsoon rainfall extent and intensity has been observed, and is
689 predicted to continue (Hsu et al., 2012). In any event, the difference between prior and
690 posterior trends in Figure 11 illustrates that the current generation hydrological models, even
691 as an ensemble, is probably not a reliable surrogate observation of long-term sub-surface
692 groundwater storage changes. GRACE observations proved valuable in improving these
693 estimates.

694

695 **5. Conclusions**

696 We presented a global water cycle reanalysis that merges four total water storage retrieval
697 products derived from GRACE observations with water balance estimates derived from an
698 ensemble of five global hydrological models, water level measurements from satellite
699 altimetry, and ancillary data. We summarise our main findings as follows:

- 700 1. The data assimilation scheme generally behaves as desired, but in hydrologically complex
701 regions the analysis can be affected by poorly constrained prior estimates and error
702 specification. The greatest uncertainties occur in regions where glacier mass loss and sub-
703 surface storage declines (may) both occur but are poorly known (e.g., northern India and
704 North-American glaciers).
- 705 2. The error in original GRACE TWS data was estimated to be around 11–12 mm over non-
706 glaciated land areas. Errors in the prior estimates of TWS changes are estimated to be 17–
707 28 mm for the five models.
- 708 3. Water storage changes in other water cycle components (seasonal snow, ice, lakes and
709 rivers) are often at least as important and uncertain as changes as sub-surface water
710 storage in reconciling the various information sources.
- 711 4. The analysis results were compared to independent river water level measurements by
712 satellite altimetry, river discharge records, remotely sensed snow water storage, and
713 independent estimates of glacier mass loss. In all cases the agreement improved or
714 remained stable compared to the prior estimates, although results varied regionally. Better

715 estimates and error specification of groundwater depletion and mountain glacier mass loss
716 are required.

- 717 5. Data assimilation achieved mass balance closure over the 2003–2012 period and
718 suggested an ocean mass increase of ca. 1.45 mm y⁻¹. This reopens some question about
719 the reasons for an apparently unexplained 0.39 mm y⁻¹ (16%) of 2.45 mm y⁻¹ satellite
720 observed sea level rise for the analysis period (Chen et al., 2013).
- 721 6. For the period 2003–2012, we estimate glaciers and polar ice caps to have lost around 572
722 Gt y⁻¹, with an additional small contribution from seasonal snow (-18 Gt y⁻¹). The net
723 change in surface water storage in large lakes and rivers was insignificant, with
724 compensating effects from new reservoir impoundments (+16 Gt y⁻¹), lowering water
725 level in the Caspian Sea (-27 Gt y⁻¹) and increases in the other lakes combined (+16 Gt y⁻¹)
726 ¹). The net change in subsurface storage was significant when considering a likely
727 misattribution of glacier mass loss, and may be as high as +202 Gt y⁻¹ when excluding
728 groundwater depletion (-92 Gt y⁻¹). Increases were mainly in northern temperate regions
729 and in the seasonally wet tropics of South America and southern Africa (+87 Gt y⁻¹).
730 Continued observation will help determine if these trends are due to transient climate
731 variability or likely to persist.

732

733 **Acknowledgements**

734 GRACE land data were processed by Sean Swenson and the ocean data by Don P. Chambers,
735 both supported by the NASA MEASURES Program, and are available at
736 <http://grace.jpl.nasa.gov>. The GLDAS and TMPA data used in this study were acquired as
737 part of the mission of NASA's Earth Science Division and archived and distributed by the
738 Goddard Earth Sciences (GES) Data and Information Services Center (DISC). Lake and
739 reservoir surface height variations were from the USDA's Global Reservoir and Lake
740 (GRLM) web site [/www.pecad.fas.usda.gov/cropexplorer/global_reservoir/](http://www.pecad.fas.usda.gov/cropexplorer/global_reservoir/), funded by
741 USDA/FAS/OGA and NASA Global Agriculture Monitoring (GLAM) Project. Altimetric
742 lake level time-series variations were from the Topex/Poseidon, Jason-1, Jason-2/OSTM, and
743 Geosat Follow-On (GFO) missions.

744

745 **References**

746 Boening, C., Willis, J. K., Landerer, F. W., Nerem, R. S., and Fasullo, J.: The 2011 La Niña:
747 So strong, the oceans fell, *Geophysical Research Letters*, 39, L19602,
748 10.1029/2012gl053055, 2012.

749 Bouttier, F., and Courtier, P.: Data assimilation concepts and methods, ECMWF
750 Meteorological Training Course Lecture Series, 14, 1999.

751 Bruinsma, S., Lemoine, J.-M., Biancale, R., and Valès, N.: CNES/GRGS 10-day gravity field
752 models (release 2) and their evaluation, *Advances in Space Research*, 45, 587-601, doi:
753 10.1016/j.asr.2009.10.012, 2010.

754 Cazenave, A., Dominh, K., Guinehut, S., Berthier, E., Llovel, W., Ramillien, G., Ablain, M.,
755 and Larnicol, G.: Sea level budget over 2003-2008: A reevaluation from GRACE space
756 gravimetry, satellite altimetry and Argo, *Global and Planetary Change*, 65, 83-88, 2009.

757 Chambers, D. P., and Bonin, J. A.: Evaluation of Release-05 GRACE time-variable gravity
758 coefficients over the ocean, *Ocean Science*, 8, 859-868, 10.5194/os-8-859-2012, 2012.

759 Chen, J. L., Wilson, C. R., and Tapley, B. D.: Contribution of ice sheet and mountain glacier
760 melt to recent sea level rise, *Nature Geoscience*, 6, 549-552, 10.1038/ngeo1829, 2013.

761 Cogley, J. G.: GGHYDRO-Global Hydrographic Data, release 2.3, Technical Note 2003-1,
762 Department of Geography, Trent University, Peterborough, Ontario, Canada, 2003 (available
763 at people.trentu.ca/gcogley/glaciology/gghrls231.pdf).

764 Crétaux, J. F., Jelinski, W., Calmant, S., Kouraev, A., Vuglinski, V., Bergé-Nguyen, M.,
765 Gennero, M. C., Nino, F., Abarca Del Rio, R., Cazenave, A., and Maisongrande, P.: SOLS: A
766 lake database to monitor in the Near Real Time water level and storage variations from
767 remote sensing data, *Advances in Space Research*, 47, 1497-1507, doi:
768 10.1016/j.asr.2011.01.004, 2011.

769 Dai, A., Qian, T., Trenberth, K. E., and Milliman, J. D.: Changes in continental freshwater
770 discharge from 1948 to 2004, *Journal of Climate*, 22, 2773-2792, 2009.

771 Dorigo, W. A., Scipal, K., Parinussa, R. M., Liu, Y. Y., Wagner, W., De Jeu, R. A. M., and
772 Naeimi, V.: Error characterisation of global active and passive microwave soil moisture
773 datasets, *Hydrology and Earth System Science*, 14, 2605-2616, 2010.

774 Fang, H., Wei, S., Jiang, C., and Scipal, K.: Theoretical uncertainty analysis of global
775 MODIS, CYCLOPES, and GLOBCARBON LAI products using a triple collocation method,
776 *Remote Sensing of Environment*, 124, 610-621, doi: 10.1016/j.rse.2012.06.013, 2012.

777 Fasullo, J. T., Boening, C., Landerer, F. W., and Nerem, R. S.: Australia's unique influence
778 on global sea level in 2010–2011, *Geophysical Research Letters*, 40, 4368-4373,
779 10.1002/grl.50834, 2013.

780 Gardner, A. S., Moholdt, G., Cogley, J. G., Wouters, B., Arendt, A. A., Wahr, J., Berthier, E.,
781 Hock, R., Pfeffer, W. T., Kaser, G., Ligtenberg, S. R. M., Bolch, T., Sharp, M. J., Hagen, J.
782 O., van den Broeke, M. R., and Paul, F.: A Reconciled Estimate of Glacier Contributions to
783 Sea Level Rise: 2003 to 2009, *Science*, 340, 852-857, 10.1126/science.1234532, 2013.

784 Geruo, A., Wahr, J., and Zhong, S.: Computations of the viscoelastic response of a 3-D
785 compressible Earth to surface loading: an application to Glacial Isostatic Adjustment in
786 Antarctica and Canada, *Geophysical Journal International*, 192, 557-572, 2013.

787 Gong, L., Halldin, S., and Xu, C. Y.: Global-scale river routing—an efficient time-delay
788 algorithm based on HydroSHEDS high-resolution hydrography, *Hydrological Processes*, 25,
789 1114-1128, 10.1002/hyp.7795, 2011.

790 Hsu, P.-C., Li, T., Luo, J.-J., Murakami, H., Kitoh, A., and Zhao, M.: Increase of global
791 monsoon area and precipitation under global warming: A robust signal?, *Geophysical
792 Research Letters*, 39, L06701, 10.1029/2012GL051037, 2012.

793 Huffman, G. J., Adler, R. F., Bolvin, D. T., Gu, G. J., Nelkin, E. J., Bowman, K. P., Hong,
794 Y., Stocker, E. F., and Wolff, D. B.: The TRMM multisatellite precipitation analysis
795 (TMPA): Quasi-global, multiyear, combined-sensor precipitation estimates at fine scales,
796 *Journal of Hydrometeorology*, 8, 38-55, 2007.

797 Jacob, T., Wahr, J., Pfeffer, W. T., and Swenson, S.: Recent contributions of glaciers and ice
798 caps to sea level rise, *Nature*, 482, 514-518, 2012.

799 Jekeli, C.: Alternative Methods to Smooth the Earth's Gravity Field. Report 327, Department
800 of Geodetic Science and Surveying, Ohio State University, Columbus, Ohio, 1981 (available
801 at www.geology.osu.edu/~jekeli.1/OSUReports/reports/report_327.pdf)

802 Landerer, F. W., and Swenson, S. C.: Accuracy of scaled GRACE terrestrial water storage
803 estimates, *Water Resources Research*, 48, W04531, 10.1029/2011WR011453, 2012.

804 Lehner, B., Liermann, C. R., Revenga, C., Vörösmarty, C., Fekete, B., Crouzet, P., Döll, P.,
805 Endejan, M., Frenken, K., Magome, J., Nilsson, C., Robertson, J. C., Rödel, R., Sindorf, N.,
806 and Wissler, D.: High-resolution mapping of the w' rld's reservoirs and dams for sustainable

807 river-flow management, *Frontiers in Ecology and the Environment*, 9, 494-502,
808 10.1890/100125, 2011.

809 Leuliette, E. W., and Miller, L.: Closing the sea level rise budget with altimetry, Argo, and
810 GRACE, *Geophysical Research Letters*, 36, L04608, 10.1029/2008gl036010, 2009.

811 Liu, Y., Weerts, A. H., Clark, M., Hendricks Franssen, H. J., Kumar, S., Moradkhani, H.,
812 Seo, D. J., Schwanenberg, D., Smith, P., van Dijk, A. I. J. M., van Velzen, N., He, M., Lee,
813 H., Noh, S. J., Rakovec, O., and Restrepo, P.: Advancing data assimilation in operational
814 hydrologic forecasting: progresses, challenges, and emerging opportunities, *Hydrology and*
815 *Earth System Science*, 16, 3863-3887, 10.5194/hess-16-3863-2012, 2012a.

816 Liu, Y. Y., Parinussa, R. M., Dorigo, W. A., De Jeu, R. A. M., Wagner, W., van Dijk, A.,
817 McCabe, M. F., and Evans, J. P.: Developing an improved soil moisture dataset by blending
818 passive and active microwave satellite-based retrievals, *Hydrology and Earth System*
819 *Science*, 15, 425-436, 2011.

820 Liu, Y. Y., Dorigo, W., Parinussa, R., De Jeu, R., Wagner, W., McCabe, M., Evans, J., and
821 Van Dijk, A.: Trend-preserving blending of passive and active microwave soil moisture
822 retrievals, *Remote Sensing of Environment*, 123, 280-297, 2012b.

823 Luojus, K., Pulliainen, J., Takala, M., Derksen, C., Rott, H., Nagler, T., Solberg, R.,
824 Wiesmann, A., Metsamaki, S., Malnes, E., and Bojkov, B.: Investigating the feasibility of the
825 globsnow snow water equivalent data for climate research purposes, *Geoscience and Remote*
826 *Sensing Symposium (IGARSS), 2010 IEEE International*, 2010,

827 Miralles, D. G., De Jeu, R. A. M., Gash, J. H., Holmes, T. R. H., and Dolman, A. J.:
828 Magnitude and variability of land evaporation and its components at the global scale,
829 *Hydrology and Earth System Science*, 15, 967-981, 10.5194/hess-15-967-2011, 2011.

830 Oki, T., and Sud, Y. C.: Design of Total Runoff Integrating Pathways (TRIP)-A global river
831 channel network, *Earth Interactions*, 2, 1-37, 1998.

832 Oki, T., Nishimura, T., and Dirmeyer, P. A.: Assessment of Annual Runoff from Land
833 Surface Models Using Total Runoff Integrating Pathways (TRIP), *Journal of Meteorology*,
834 77, 235-255, 1999.

835 Peña-Arancibia, J., Van Dijk, A. I. J. M., Mulligan, M., and Renzullo, L. J.: Evaluation of
836 precipitation estimation accuracy in reanalyses, satellite products and an ensemble method for

837 regions in Australia and in south and east Asia, *Journal of Hydrometeorology* 14, 1323-1333,
838 2013.

839 Pulliainen, J.: Mapping of snow water equivalent and snow depth in boreal and sub-arctic
840 zones by assimilating space-borne microwave radiometer data and ground-based
841 observations, *Remote Sensing of Environment*, 101, 257-269, doi: 10.1016/j.rse.2006.01.002,
842 2006.

843 Rodell, M., Houser, P., Jambor, U., Gottschalck, J., Mitchell, K., Meng, C., Arsenault, K.,
844 Cosgrove, B., Radakovich, J., and Bosilovich, M.: The global land data assimilation system,
845 *Bulletin American Meteorological Society*, 85, 381-394, 2004.

846 Rui, H.: README Document for Global Land Data Assimilation System Version 1
847 (GLDAS-1) Products, NASA, 2011 (available at
848 http://hydro1.sci.gsfc.nasa.gov/data/s4pa/NLDAS/NLDAS_FOR0125_H.001/doc/README.NLDAS1.pdf)
849 NLDAS1.pdf)

850 Sakumura, C., Bettadpur, S., and Bruinsma, S.: Ensemble prediction and intercomparison
851 analysis of GRACE time-variable gravity field models, *Geophysical Research Letters*, 41,
852 1389-1397, 10.1002/2013GL058632, 2014.

853 Scipal, K., Holmes, T., de Jeu, R., Naeimi, V., and Wagner, W.: A possible solution for the
854 problem of estimating the error structure of global soil moisture data sets, *Geophysical*
855 *Research Letters*, 35, 2009.

856 Sheffield, J., Goteti, G., and Wood, E. F.: Development of a 50-year high-resolution global
857 dataset of meteorological forcings for land surface modeling, *Journal of Climate*, 19, 3088-
858 3111, 2006.

859 Sheffield, J., Wood, E. F., and Roderick, M. L.: Little change in global drought over the past
860 60 years, *Nature*, 491, 435-438, 2012.

861 Stoffelen, A.: Toward the true near-surface wind speed: Error modeling and calibration using
862 triple collocation, *Journal of Geophysical Research: Oceans*, 103, 7755-7766,
863 10.1029/97jc03180, 1998.

864 Swenson, S., and Wahr, J.: Post-processing removal of correlated errors in GRACE data,
865 *Geophysical Research Letters*, 33, L08402, 10.1029/2005gl025285, 2006.

866 Swenson, S., Famiglietti, J., Basara, J., and Wahr, J.: Estimating profile soil moisture and
867 groundwater variations using GRACE and Oklahoma Mesonet soil moisture data, *Water*
868 *Resources Research*, 44, W01413, 10.1029/2007wr006057, 2008.

869 Takala, M., Pulliainen, J., Metsamäki, S. J., and Koskinen, J. T.: Detection of Snowmelt
870 Using Spaceborne Microwave Radiometer Data in Eurasia From 1979 to 2007, *Geoscience*
871 *and Remote Sensing, IEEE Transactions on*, 47, 2996-3007, 10.1109/TGRS.2009.2018442,
872 2009.

873 Tapley, B. D., Bettadpur, S., Ries, J. C., Thompson, P. F., and Watkins, M. M.: GRACE
874 Measurements of Mass Variability in the Earth System, *Science*, 305, 503-505,
875 10.1126/science.1099192, 2004.

876 Tregoning, P., McClusky, S., van Dijk, A., Crosbie, R. S., and Peña-Arancibia, J. L.:
877 Assessment of GRACE satellites for groundwater estimation in Australia, *National Water*
878 *Commission, Canberra*, 82, 2012 (available at archive.nwc.gov.au/library/waterlines/71).

879 Van Dijk, A. I. J. M.: Model-data fusion: Using observations to understand and reduce
880 uncertainty in hydrological models, In: *Proceedings, MODSIM 2011, 12-16 December 2011,*
881 *Perth, 2011.*

882 Van Dijk, A. I. J. M., and Renzullo, L. J.: Water resource monitoring systems and the role of
883 satellite observations, *Hydrology and Earth System Sciences*, 15, 39-55, 10.5194/hess-15-39-
884 2011, 2011.

885 Van Dijk, A. I. J. M., Renzullo, L. J., and Rodell, M.: Use of Gravity Recovery and Climate
886 Experiment terrestrial water storage retrievals to evaluate model estimates by the Australian
887 water resources assessment system, *Water Resources Research*, 47, W11524.,
888 10.1029/2011WR010714, 2011.

889 Van Dijk, A. I. J. M., Peña-Arancibia, J. L., Wood, E. F., Sheffield, J., and Beck, H. E.:
890 Global analysis of seasonal streamflow predictability using an ensemble prediction system
891 and observations from 6192 small catchments worldwide, *Water Resources Research*, doi:
892 10.1002/wrcr.20251, 10.1002/wrcr.20251, 2013.

893 Vörösmarty, C. J., and Moore III, B. I.: Modeling basin-scale hydrology in support of
894 physical climate and global biogeochemical studies: An example using the Zambezi River,
895 *Surveys in Geophysics*, 12, 271-311, 10.1007/bf01903422, 1991.

896 Wada, Y., van Beek, L. P. H., van Kempen, C. M., Reckman, J. W. T. M., Vasak, S., and
897 Bierkens, M. F. P.: Global depletion of groundwater resources, *Geophysical Research*
898 *Letters*, 37, L20402, 10.1029/2010gl044571, 2010.

899 Wada, Y., van Beek, L. P. H., Sperna Weiland, F. C., Chao, B. F., Wu, Y.-H., and Bierkens,
900 M. F. P.: Past and future contribution of global groundwater depletion to sea-level rise,
901 *Geophysical Research Letters*, 39, L09402, 10.1029/2012GL051230, 2012.

902 Wada, Y., Van Beek, R., Wanders, N., and Bierkens, M. F. P.: Human water consumption
903 intensifies hydrological drought worldwide, *Environmental Research Letters*, 8, 034036,
904 2013.

905 Wahr, J., Swenson, S., and Velicogna, I.: Accuracy of GRACE mass estimates, *Geophysical*
906 *Research Letters*, 33, L06401, 10.1029/2005GL025305, 2006.

907 Wang, X., de Linage, C., Famiglietti, J., and Zender, C. S.: Gravity Recovery and Climate
908 Experiment (GRACE) detection of water storage changes in the Three Gorges Reservoir of
909 China and comparison with in situ measurements, *Water Resources Research*, 47, 2011.

910 Zaitchik, B. F., Rodell, M., and Reichle, R. H.: Assimilation of GRACE Terrestrial Water
911 Storage Data into a Land Surface Model: Results for the Mississippi River Basin, *Journal of*
912 *Hydrometeorology*, 9, 535-548, doi:10.1175/2007JHM951.1, 2008.

913 Zwieback, S., Scipal, K., Dorigo, W., and Wagner, W.: Structural and statistical properties of
914 the collocation technique for error characterization, *Nonlinear Processes in Geophysics*, 19,
915 69-80, 2012.

916

917

918 Table 1. Description and sources of data used in this analysis. Acronyms are explained in the
 919 text.

Description	Source	Data access
<i>Prior estimates</i>		
model estimates (CLM, MOS, NOAH, VIC)	GLDAS	ftp://hydro1.sci.gsfc.nasa.gov/data/s4pa/GLDAS_V1/ (data accessed 17 April 2013).
Model estimates (W3RA)		available from author Van Dijk
groundwater depletion		available from author Wada
river flow direction	TRIP	http://hydro.iis.u-tokyo.ac.jp/~taikan/TRIPDATA/Data/trip05.asc (downloaded 10 May 2013)
discharge from small catchments		available from author Van Dijk
discharge from large basins		http://www.cgd.ucar.edu/cas/catalog/surface/dai-runoff/index.html
surface water extraction		available from author Wada
lake water level	Crop Explorer	http://www.pecad.fas.usda.gov/cropexplorer/global_reservoir/ (downloaded 9 May 2013)
new dam impoundments	GranD	http://atlas.gwsp.org/ (accessed 14 May 2014)
new dam impoundments	ICOLD	http://www.icold-cigb.org/ (accessed 14 May 2014)
sea level	AVISO	http://www.aviso.oceanobs.com/en/data/products/sea-surface-height-products/global/ (downloaded 7 November 2013)
glacier extent	GGHYDRO	http://people.trentu.ca/~gcogley/glaciology/ (downloaded 12 June 2013)
<i>Assimilated data</i>		
TWS: CSR, GFZ, JPL	Tellus	ftp://podaac-ftp.jpl.nasa.gov/allData/tellus/L3/land_mass/RL05/netcdf/ (downloaded 16 April 2013)
TWS: GRGS	CNES	http://grgs.obs-mip.fr/grace/variable-models-grace-lageos/grace-solutions-release-02 (downloaded 16 April 2013)
glacial isostatic adjustment	Tellus	ftp://podaac-ftp.jpl.nasa.gov/allData/tellus/L3/land_mass/RL05/netcdf/ (downloaded 16 April 2013)
<i>Evaluation data</i>		
water level in large rivers	LEGOS HYDROWEB	http://www.legos.obs-mip.fr/en/soa/hydrologie/hydroweb/ (downloaded 13 October 2013)
<i>idem</i>	ESA River&Lake	http://tethys.eaprs.cse.dmu.ac.uk/RiverLake/shared/main (downloaded 25 October 2012)
snow water equivalent	GLOBSNOW	http://www.globsnow.info/swe/archive_v1.3/ (downloaded 9 October 2013)

921 Table 2. Spatial mean values (non-glaciated land areas only) of the error in monthly mass
 922 change estimates for different GRACE and model sources as derived through triple
 923 collocation. Also listed is the number of triple collocation estimates derived (N) and the
 924 spatial mean of the coefficient of variation (C.V.) in these N estimates.

	Mean error	Mean C.V.	N
	mm	%	
<i>GRACE</i>			
GRG	14.3	15	15
CSR	12.8	15	5
GFZ	15.5	11	5
JPL	15.2	12	5
Merged	13.5	–	–
<i>Models</i>			
CLM	26.7	6	3
MOS	21.9	7	3
NOAH	16.6	9	3
VIC	27.7	6	3
W3RA	17.9	7	3
Merged	18.1	–	–

925

926

927 Table 3. Calculated linear trends in global mean seasonally-adjusted anomalies associated
 928 with different water cycle components for 2003–2012. The posterior trend estimates are also
 929 expressed in equivalent sea level rise (SLR) and volume. Second number is standard
 930 deviation.

Store	Prior	Posterior		
	global mean	global mean	SLR	Volume
	mm y ⁻¹	mm y ⁻¹	mm y ⁻¹	km ³ y ⁻¹
Sub-surface	-0.572 ± 0.029	0.017 ± 0.023	0.024 ± 0.032	9 ± 12
Rivers	0.012 ± 0.009	0.003 ± 0.01	0.004 ± 0.014	1 ± 5
Lakes	-0.012 ± 0.005	-0.021 ± 0.005	-0.029 ± 0.006	-11 ± 2
New dams	0.043 ± 0.001	0.032 ± 0.002	0.045 ± 0.003	16 ± 1
Seasonal snow	-0.022 ± 0.007	-0.035 ± 0.007	-0.049 ± 0.01	-18 ± 4
Arctic glaciers (>55°N)	0.265 ± 0.004	-0.604 ± 0.009	-0.849 ± 0.013	-308 ± 5
Antarctic glaciers (>55°S)	-	-0.301 ± 0.007	-0.423 ± 0.01	-154 ± 4
Remaining glaciers	-0.029 ± 0.004	-0.061 ± 0.003	-0.086 ± 0.004	-31 ± 2
Total terrestrial	-	-0.97 ± 0.035	-1.364 ± 0.049	-495 ± 18
Oceans	1.309 ± 0.044	1.029 ± 0.039	1.446 ± 0.054	525 ± 20

931

932

933

934 Table 4. Evaluation of alternative estimates of mean basin discharge using observations
935 collated by Dai et al. (2009). Listed is the agreement for the ensemble models (without bias
936 correction), the merged prior estimate and the posterior estimates resulting from reanalysis.

	CLM	MOS	NOAH	VIC	W3RA	prior	posterior
Combined discharge (km ³ y ⁻¹)	21,874	9,003	11,474	13,666	16,518	18,663	20,149
Diff. total (%)	5	-57	-45	-35	-21	-11	-4
RMSE (km ³ y ⁻¹)	114	184	126	147	63	47	44
Median % diff.	60	63	57	48	61	40	41

937

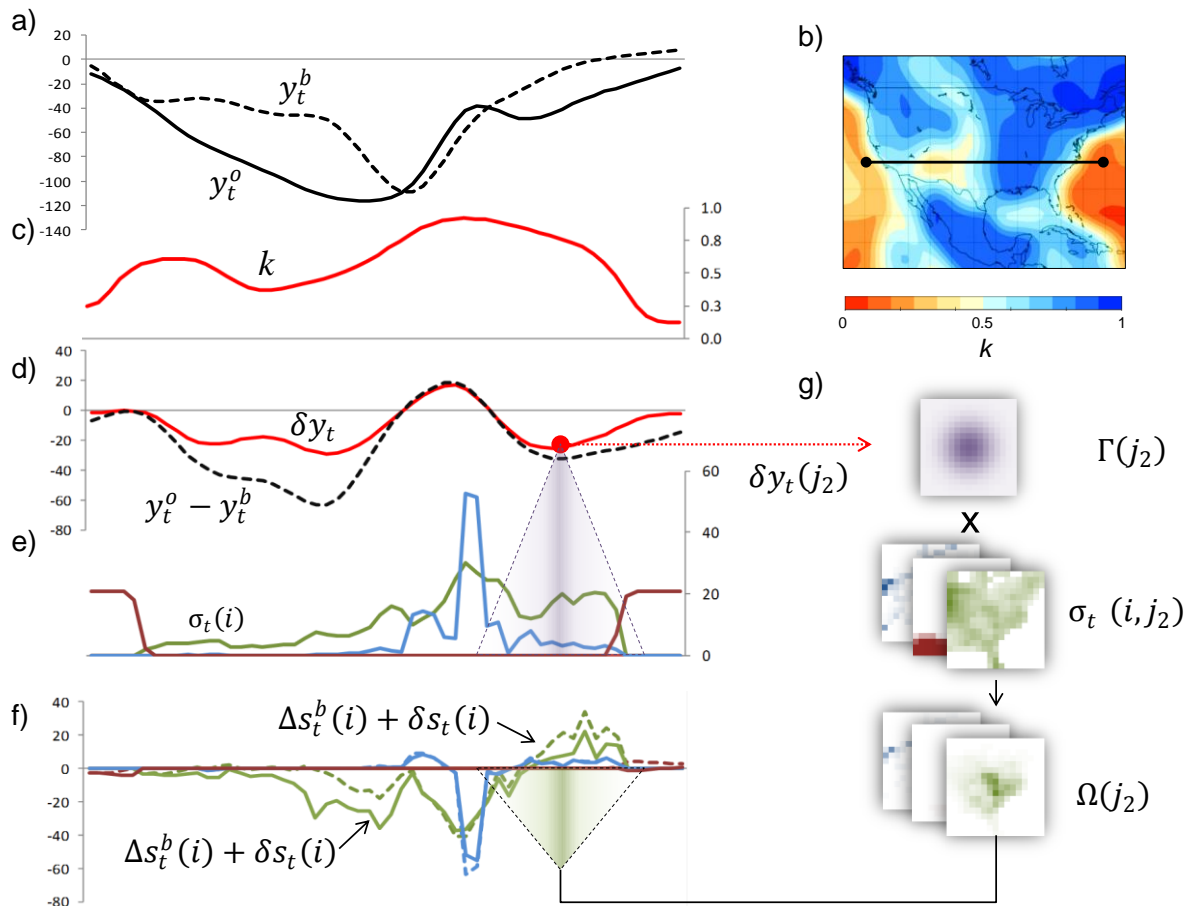
938

939

940 Table 5. Published trends in glacier water storage (Gardner et al., 2013; Jacob et al., 2012)
 941 compared to estimates from reanalysis. Uncertainties are given at the 95% (2 standard
 942 deviation) interval, superscripts refer to estimates derived from GRACE (g) or independent
 943 methods (i). Also listed are regional trends attributed to other parts of the hydrological cycle,
 944 and the ratio of the relative magnitude of that residual trends over estimated glacier mass
 945 change.

Region	Reported		This study		ratio (%)
	trend (Gt y ⁻¹)		glacier trend (Gt y ⁻¹)	other components (Gt y ⁻¹)	
Greenland ice sheet + PGICs	-222 ± 9	^g	-203 ± 10	-5 ± 1	3
Canadian Arctic Archipelago	-60 ± 6	^{i,g}	-48 ± 3	-19 ± 2	39
Alaska	-50 ± 17	^{i,g}	-23 ± 6	-23 ± 6	101
Northwest America excl. Alaska	-14 ± 3	ⁱ	3 ± 3	-8 ± 9	275
Iceland	-10 ± 2	^{i,g}	-6 ± 1	-0.6 ± 0.2	10
Svalbard	-5 ± 2	^{i,g}	-2 ± 1	0.1 ± 0.1	3
Scandinavia	-2 ± 0	ⁱ	0.4 ± 1.0	5 ± 2	>500
Russian Arctic	-11 ± 4	^{i,g}	-4 ± 1	2 ± 2	47
High Mountain Asia	-26 ± 12	^{i,g}	-29 ± 4	-15 ± 11	51
South America excl. Patagonia	-4 ± 1	ⁱ	-2 ± 1	-21 ± 33	>500
Patagonia	-29 ± 10	^g	-15 ± 1	1 ± 2	4
Antarctica ice sheet + PGICs	-165 ± 72	^g	-139 ± 8	0	0
Rest of world	-4 ± 0		-3 ± 1	82 ± 107	>500
Total	-602 ± 77		-471 ± 25		

946



947

948

949

950

951

952

953

954

955

956

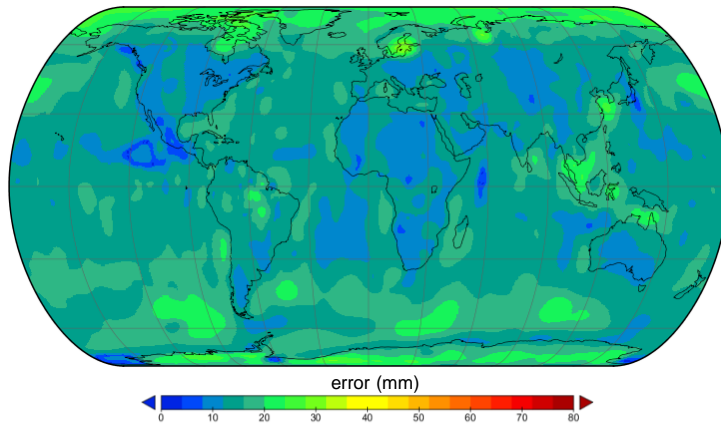
957

958

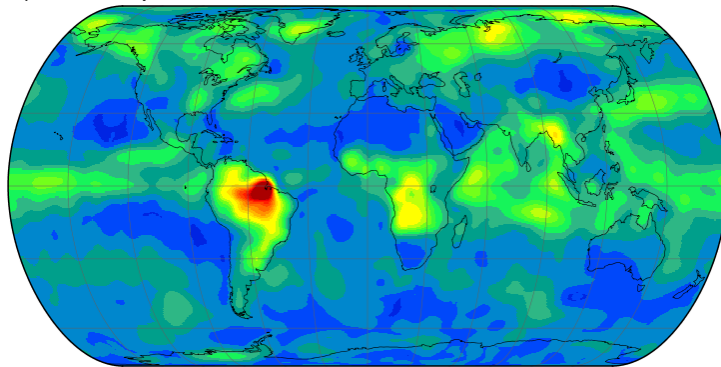
Figure 1. Illustration of the data assimilation approach followed using data along a transect through the USA for August 2003. Shown are: a) monthly satellite-derived TWS, y_t^o , and the equivalent prior estimate, y_t^b ; b) location of the West-East transect on a map of the gain matrix, k ; c) profile of k along the transect (cf. Figure 2c); d) calculation of the TWS analysis increment, δy_t , from k and innovation, $(y_t^o - y_t^b)$; e) the prior error in the change of each of the stores, $\sigma_t(i)$; f) the prior and posterior estimate of change in each store, $\Delta s_t^b(i)$ and $\Delta s_t^b(i) + \delta s_t(i)$, resp.; and g) visual illustration of the disaggregation of the TWS analysis increments to the different stores. All units are in mm unless indicated otherwise; see text for full explanation of symbols; stores shown include the sub-surface (green), rivers (blue) and sea (dark red; remaining stores not shown for clarity).

958

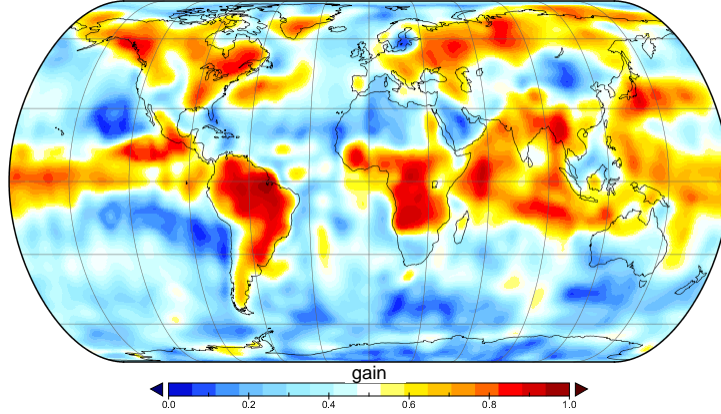
a) Error in GRACE



b) Error in prior



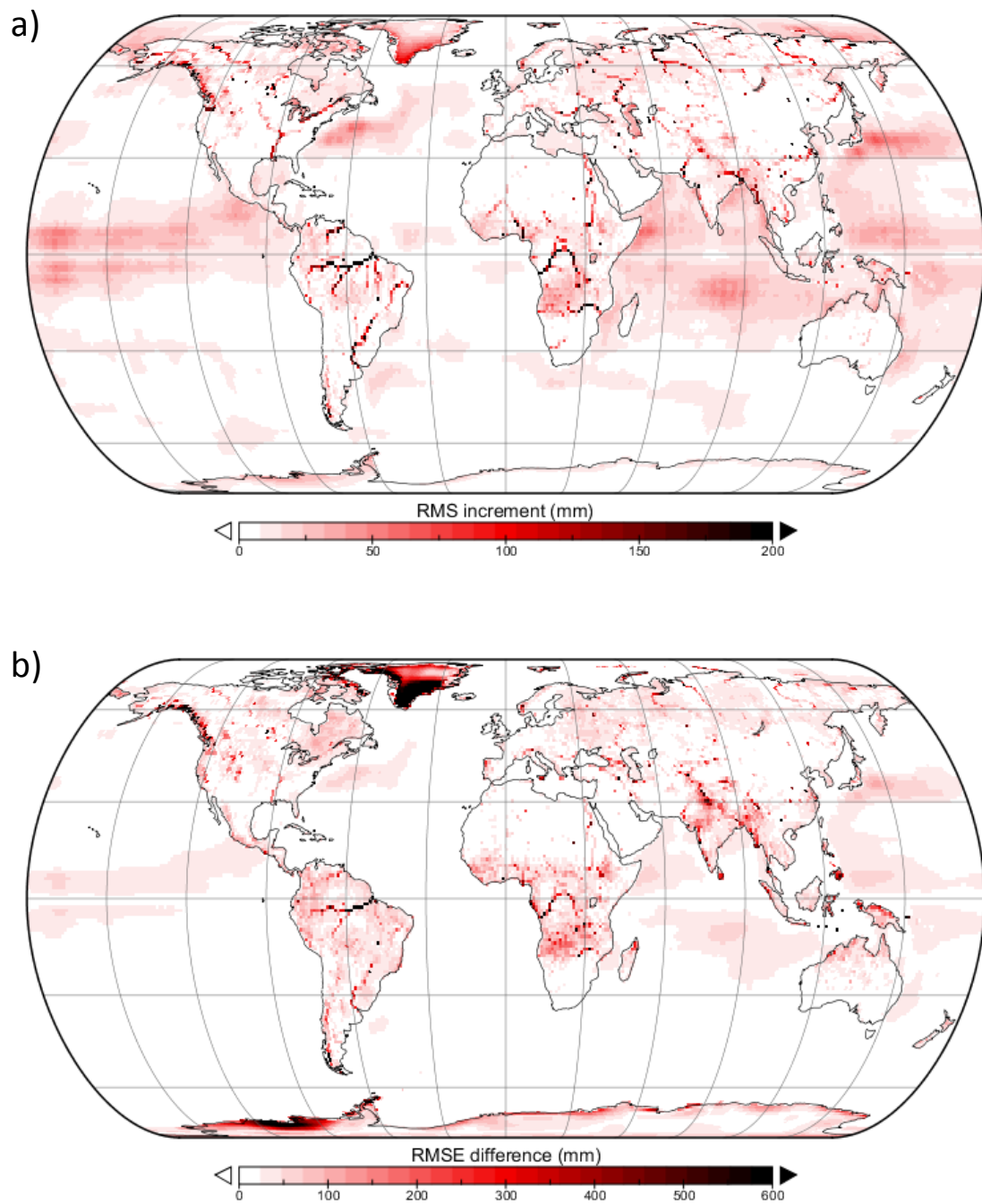
c) Gain



959

960 Figure 2. Triple collocation estimated error in storage change from the merged (a) GRACE
961 and (b) prior estimates, and (c) resulting gain matrix.

962

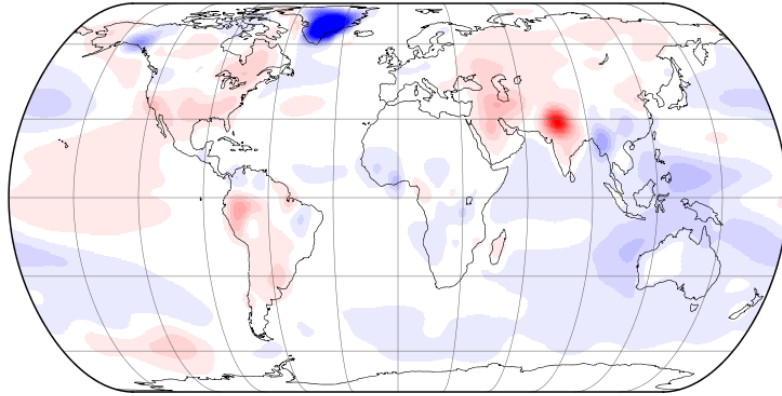


963

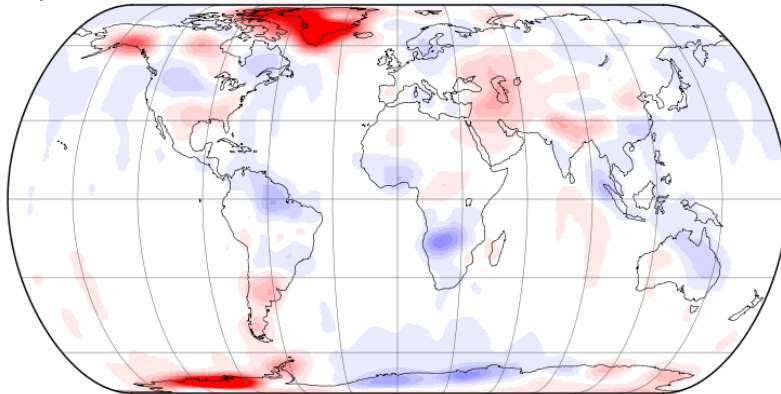
964 Figure 3. The impact of GRACE data assimilation on total water storage expressed as (a) the
 965 root mean square (RMS) analysis increment and (b) the RMS difference between prior and
 966 posterior storage time series.

967

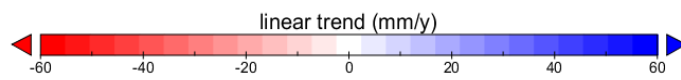
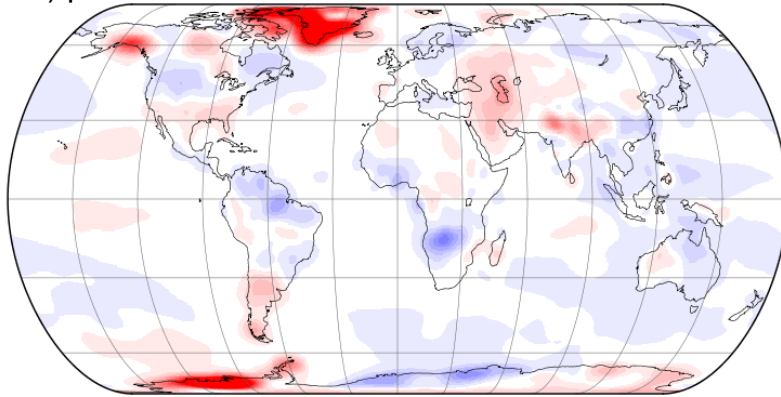
a) prior



b) GRACE



c) posterior

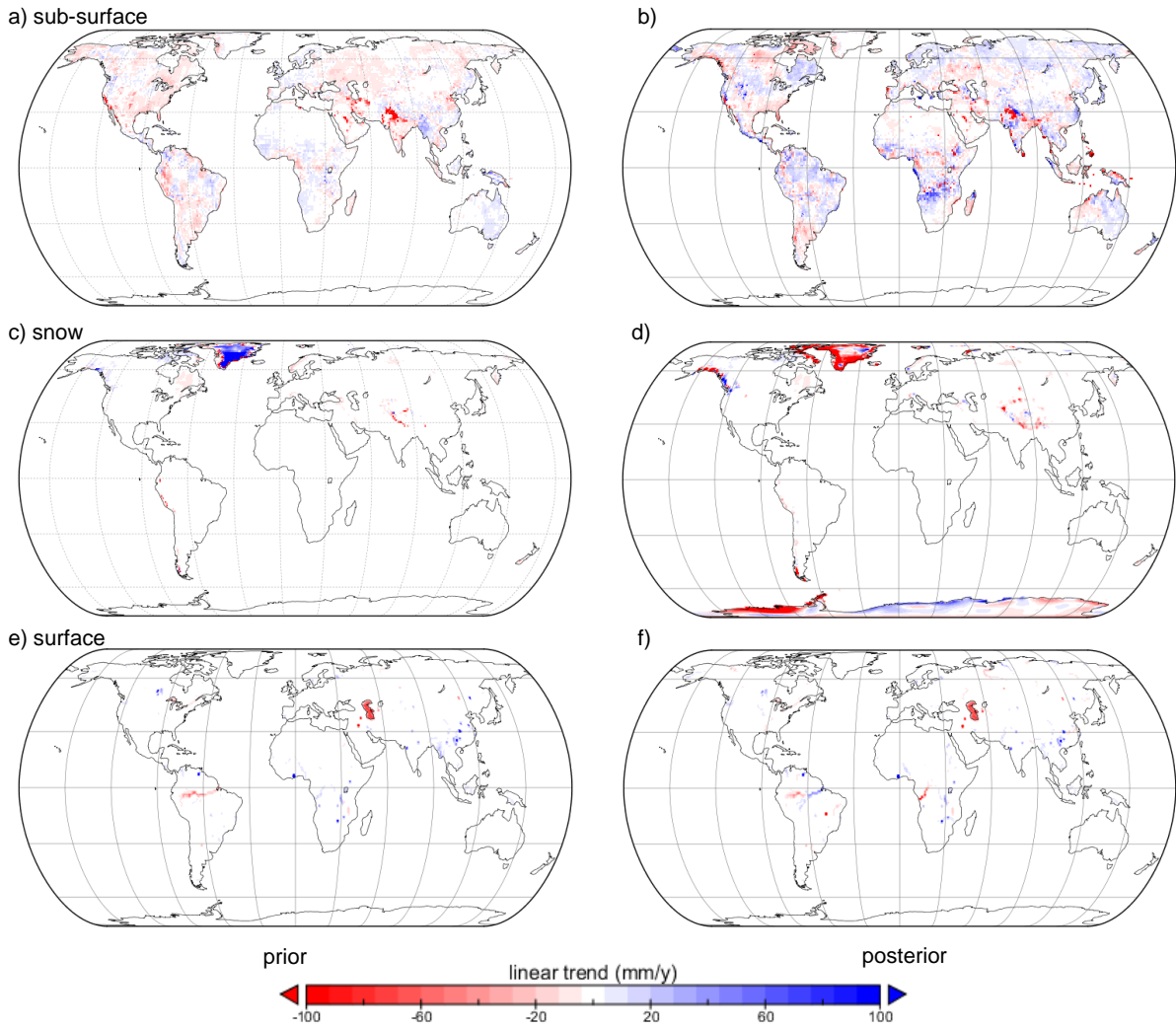


968

969 Figure 4. Trends in GRACE total water storage as derived from (a) prior storage estimates;

970 (b) merged satellite retrievals; and (c) posterior estimates.

971



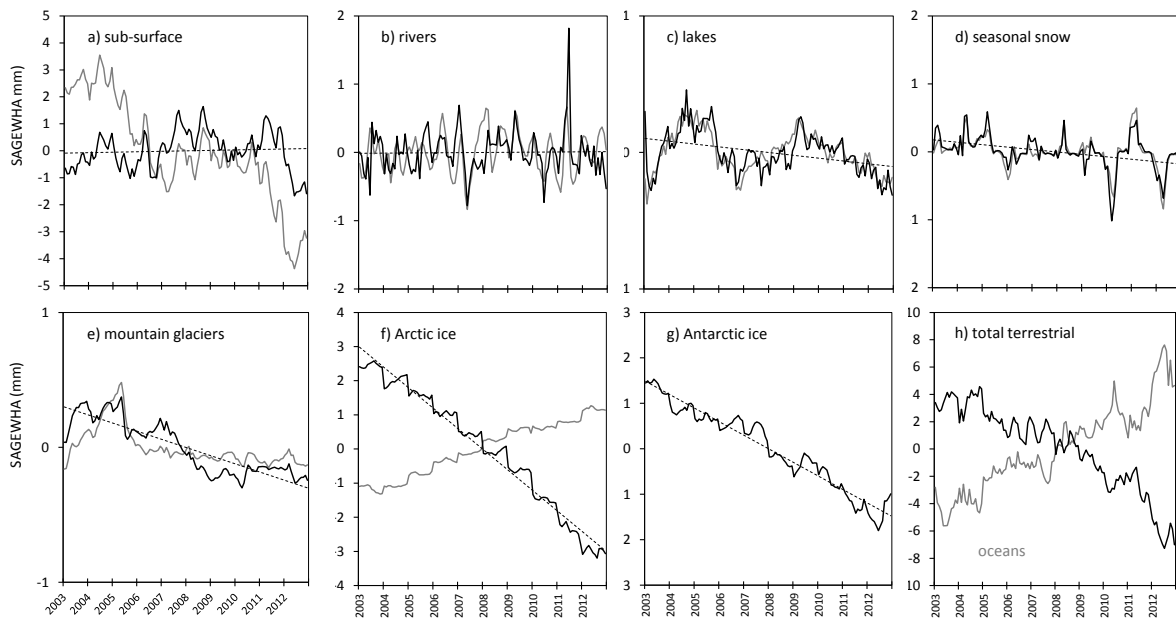
972

973 Figure 5. Trends in seasonal anomalies of prior (left column) and posterior (right column)

974 estimates of (a-b) sub-surface, (c-d) snow and (e-f) surface water (i.e., lake and river) water

975 storage.

976

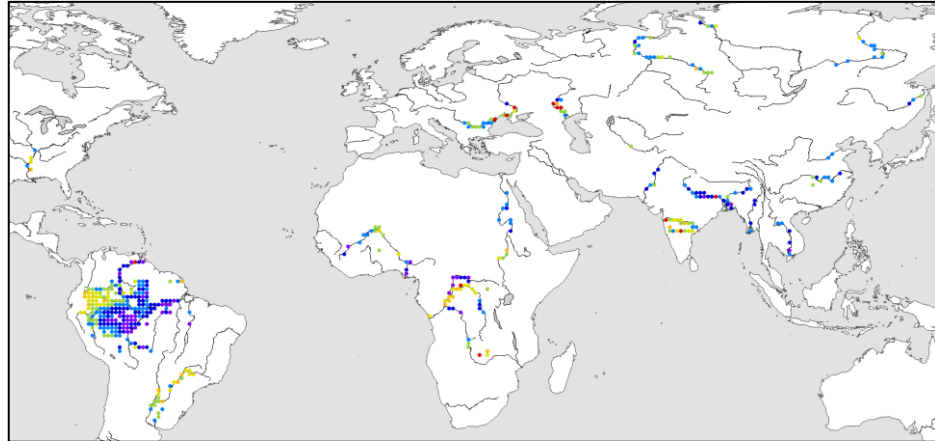
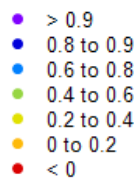


978

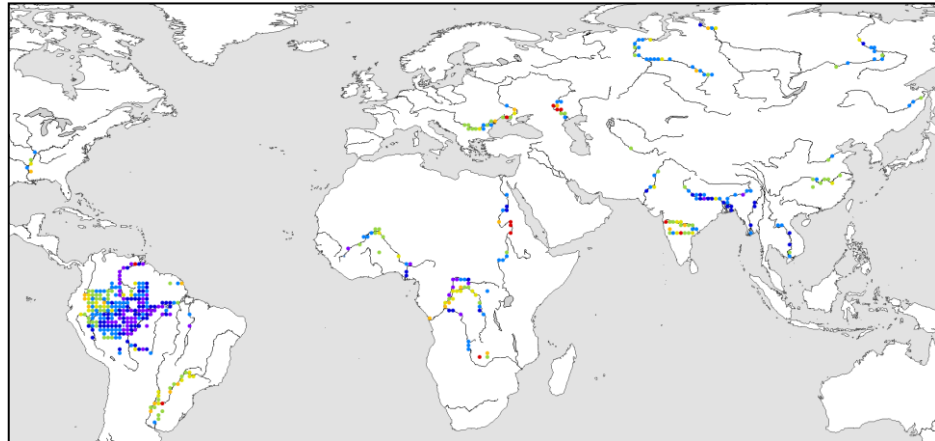
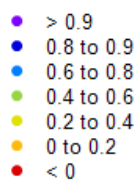
979 Figure 6. Time series of the prior (grey lines) and posterior (black lines) estimates of global
 980 average seasonally-adjusted storage anomalies in different water cycle components. Dashed
 981 lines show linear trends for 2003–2012 as listed in Table 3.

982

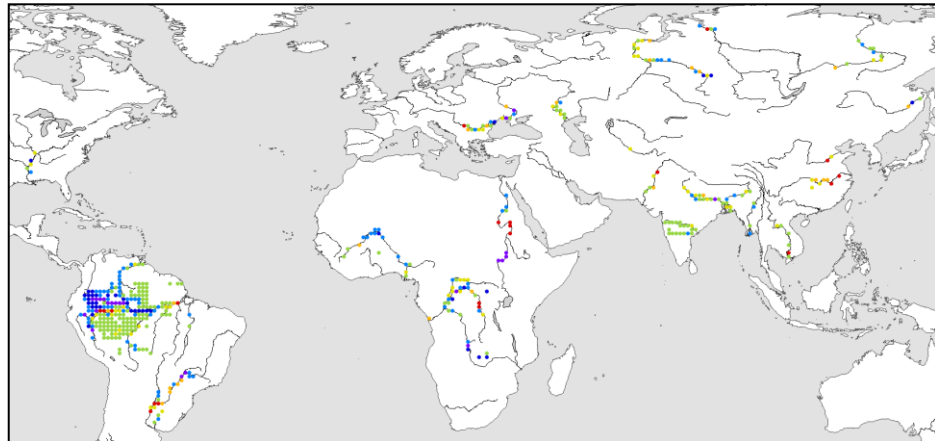
a) prior



b) posterior



c) change



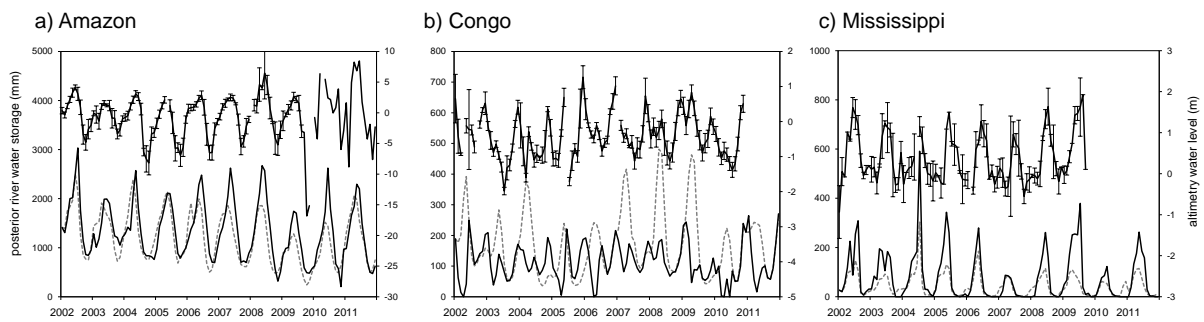
983

984 Figure 7. Effect of assimilation agreement with satellite altimetry river water levels:

985 Spearman's rank correlation coefficient (ρ) for (a) prior and (b) posterior estimates and (c)

986 difference between the two.

987

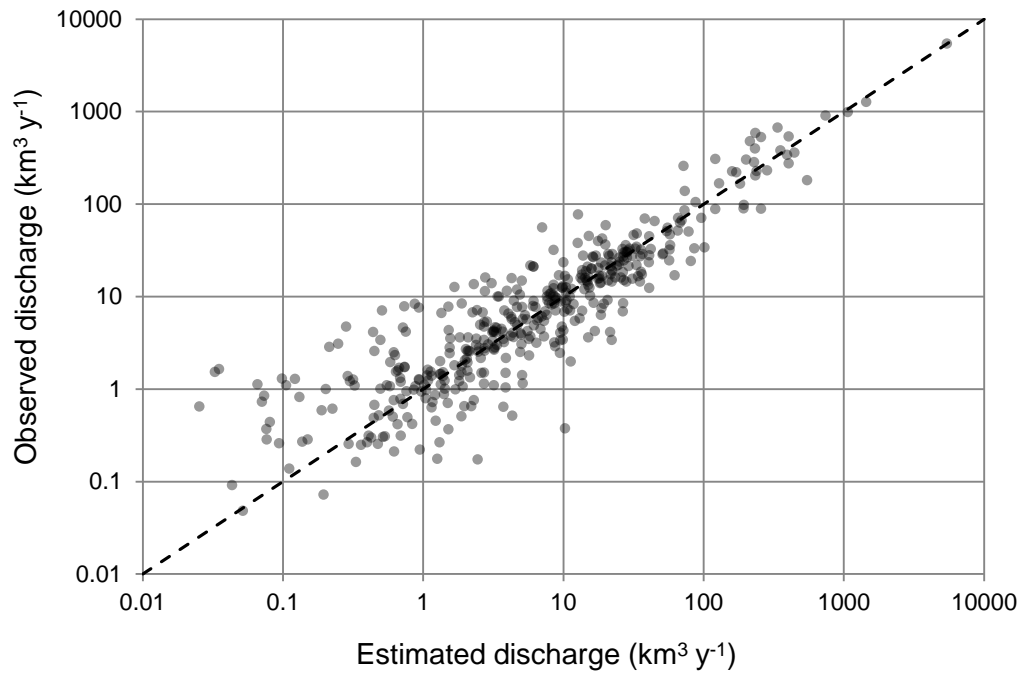


989

990 Figure 8. Effect of assimilation agreement with satellite altimetry river water levels for grid
 991 cells including the a) Amazon River ($\sim 2.5^{\circ}\text{S}$, 65.5°W ; ρ changed from 0.71 for prior to 0.80
 992 for posterior estimates); b) Congo River ($\sim 2.5^{\circ}\text{N}$, 21.5°E ; ρ from 0.28 to 0.47) and
 993 Mississippi River (35.5° , 90.5°W ; ρ from 0.37 to 0.56).

994

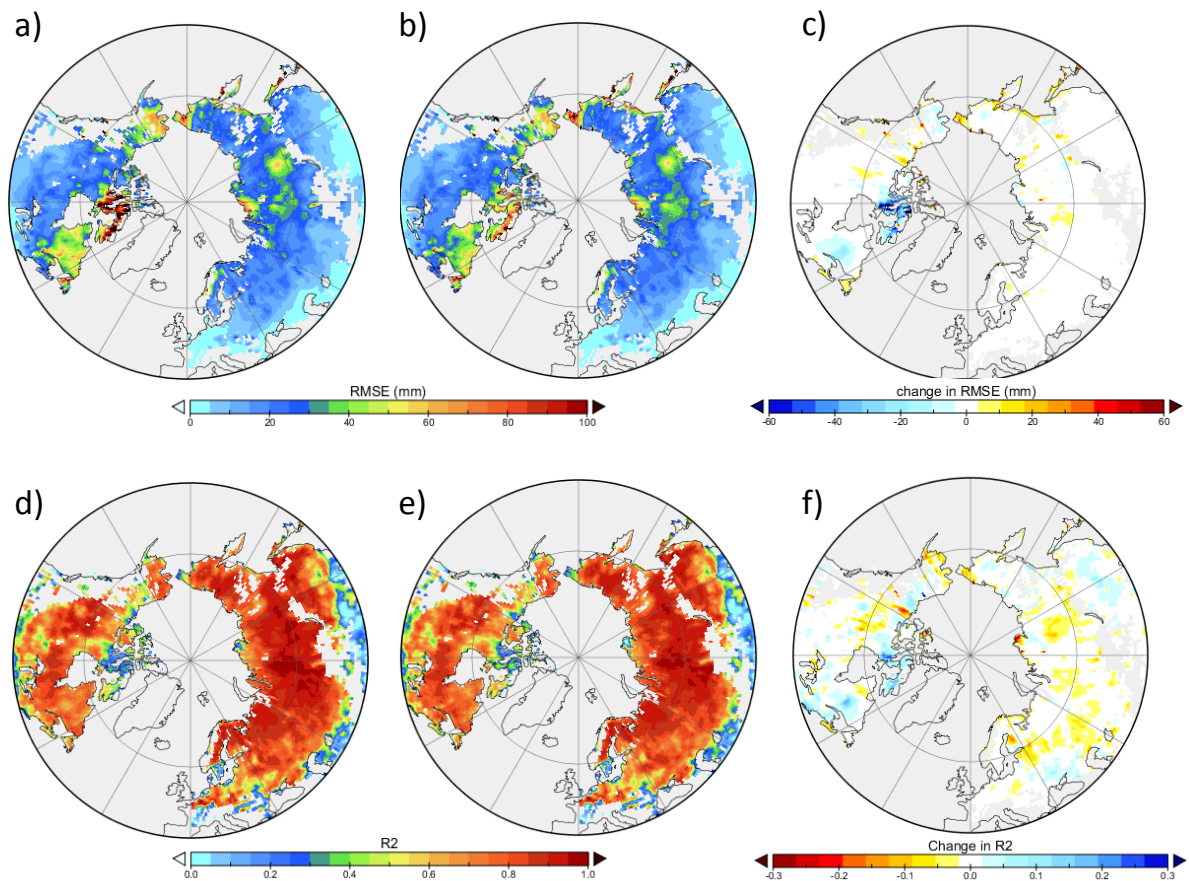
995



996

997 Figure 9. Comparison of mean basin discharge resulting from the analysis (Q_a) and values
998 based on observations (Dai et al., 2009) (darker areas indicate overlapping data points).

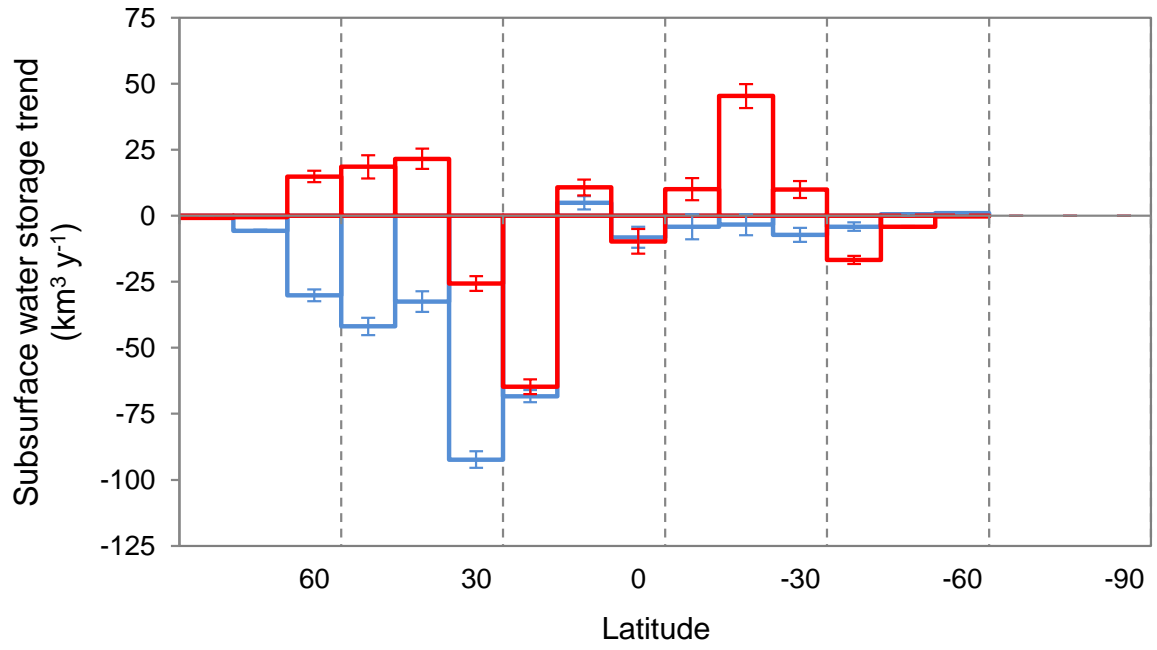
999



1000

1001 Figure 10. Effect of assimilation on agreement with GlobSnow snow water equivalent
 1002 estimates, showing (a-c) root mean square error (RMSE) and (d-f) the coefficient of
 1003 correlation (R^2). From left to right, agreement for (a,d) prior and (b, e) posterior estimates as
 1004 well as (c, f) the change in agreement.

1005



1006

1007 Figure 11. Linear 2003–2012 trends in sub-surface water storage by 10° latitude band,
 1008 showing prior (blue) and posterior (red) estimates.

1009